ORBIT DETERMINATION OF SUNLIGHT
ILLUMUNATED OBJECTS DETECTED BY
OVERHEAD PLATFORMS

THESIS

Richard P. Osedacz
Captain, USAF

AFIT/GA/ENY/89J-3

DEPARTMENT OF THE AIR FORCE
**AIR UNIVERSITY**

# AIR FORCE INSTITUTE OF TECHNOLOGY

Wright-Patterson Air Force Base, Ohio

89   6   19   072

ORBIT DETERMINATION OF SUNLIGHT
ILLUMUNATED OBJECTS DETECTED BY
OVERHEAD PLATFORMS

THESIS

Richard P. Osedacz
Captain, USAF

AFIT/GA/ENY/89J-3

AFIT/GA/ENY/89J-3

Orbit Determination of Sunlight Illuminated Objects

Detected by Overhead Platforms

THESIS

Presented to the Faculty of the School of Engineering

of the Air Force Institute of Technology

Air University

In Partial Fulfillment of the

Requirements for the Degree of

Master of Science in Astronautical Engineering

Richard P. Osedacz, B.S.

Captain, USAF

June 1989

| Accession For | |
|---|---|
| NTIS GRA&I | ☑ |
| DTIC TAB | ☐ |
| Unannounced | ☐ |
| Justification | |
| By | |
| Distribution/ | |
| Availability Codes | |
| Dist | Avail and/or Special |
| A-1 | |

## Acknowledgements

I am deeply indebted to a number of people for all of the help and support in performing this project. First of all I would like to thank Dr. Wiesel and Capt Bain for their never ending support and patience when the going got tough. I also wish to thank the members of the Powered Flight Group, Flight Performance Division of the Foreign Technology Division for sponsoring me in this task. In particular I would like to thank Ed Creehan for getting me started on this project, Larry Lillard who coached me in the intricacies of estimation theory applied to trajectory reconstruction, Jim Bernier from Geodynamics Corporation for stimulating my interest in trajectory estimation and its other applications and the class of GA-89D for keeping my spirits up during dark and gloomy times. Finally I am extremely grateful to my wife Carol for her understanding and support during those long hours which was spent with the computer instead of her.

i

# Table of Contents

iii

## List of Figures

iv

## List of Tables

# Abstract

A technique for determining the orbital element set of a sunlight-illuminated object detected by an overhead platform (when passing through the sensor's field of view) is developed. The technique uses a Gauss orbit determination technique to find an initial target state estimate and then the estimate is refined via a batch weighted least squares estimation routine. A six element state vector consisting of three position and three velocity components describe the state at epoch. It was found that the Gaussian method produced reasonable initial orbits when the data bias was sufficiently zero. Each analyst-supplied slant range fit the data equally well, indicating that orbit determination is impossible with a single set of data. A unique series of events where the same object was tracked four consecutive days was fit using the developed algorithm, producing favorable results. The results of two single data set events and one multiple collection events are presented.

vi

# Orbit Determination of Sunlight-Illuminated Objects
## Detected by Overhead Platforms

## I. Introduction

### Objective and Scope

Due to the multitude of objects in the geostationary belt, overhead platforms are being saturated by reflected sunlight from orbiting objects passing through the sensors' field of view. These objects, known as fastwalkers, are creating a suspicion that some uncatalogued objects may exist or are being cross-tagged within the data base. The North American Aerospace Defense Command (NORAD) tasked the Foreign Technology Division, Flight Performance Division (FTD/SQDF) to analyze these 15 to 30 minute data tracks and determine the element set, identifying the object.

The objective of this thesis is twofold: to determine the feasibility of determining the element set of an orbiting object from space-based metric data and if so, perform a commonality/occurrence frequency study of a year's worth of collected data. The project can be expanded to warn the sensor operator when the next occurrence will be so that he can take preventative measures to protect the sensor from damaging cell over-saturation.

1

In order to start the analysis, a few underlying assumptions must be made. First, the sensor ephemerides are known exactly, since this is the best true baseline information available. Also, sensor location is a type of Q-parameter, where Q-parameters are defined by Day as those parameters which effect the observations but, for some reason, cannot be estimated (5:3-1). Other examples of Q-parameters are atmospheric density, data biases, and the like. P-parameters, on the other hand, are those parameters which can be estimated from the given data.

Secondly, the objects (targets) are assumed to be non-thrusting bodies within 1000 km from the sensor since the collected data tracks can be as long as 30 minutes, implying that the object's orbital speed is nearly the same as the sensor's orbital speed. This assumption along with the fact that orbital perturbations will have no visible effect on the target during the span of the data track, the two body equations of motion will be sufficient to estimate the orbital element set.

The simulated data for this project were generated by the Modularized Vehicle Simulation/Trajectory Reconstruction Program (MVS/TRP), a batch weighted least squares estimator originally developed to validate the guidance equations of various space boosters. The data were generated with $1-\sigma$ Gaussian white noise at one point every ten seconds.

2

**Table I    Description of Simulated Test Case Data**

| Data Rate: 1pt/10 sec |
| :---: |
| Nominal 1-$\sigma$ Data Errors |
| Azimuth: 3.5 X $10^{-5}$        Elevation: 4.3 X $10^{-6}$ |

## Research

Since the fastwalker data base goes back as far as 1972, it is safe to assume that the problem has been in existence since then.   It is most prevalent with a certain ballistic missile early warning satellite system located at various geostationary locations.   Wong in his paper performed his analysis using various intensity models and a least squares estimator (MVS/TRP) to find that there is a family of least squares solutions in r which satisfy the collected azimuth and elevation data (21:23-25).   Little was done to resolve this family into a single possible fastwalker, hence his conclusion was that the problem was unsolvable.

Some undocumented simulations were performed in the Space Surveillance Center within the NORAD Cheyenne Mountain Complex where the sensor was boosted into a higher orbit and then circularized 500 km above its original position.   Then based on the viewing angle a collection of other satellites in its

3

field of view were listed at a particular epoch time. This proved to be futile in singling out one particular satellite as the fastwalker. Other than the above mentioned instances, no other work has been performed on fastwalker analysis.

## Approach

Since pure angular data is given along with the sensor ephemeris over the data span, the Gauss orbit determination method will be used to determine an intial orbit. The initial target (fastwalker) state vector can then be refined with a batch weighted least squares estimator to further update the orbit.

The ephemeris is reported in latitude, longitude, altitude and time since no velocity information is required to fit the data (i.e. the data is also position related. No doppler or other velocity related effects need to be taken into account to correct the data model). However, an accurate velocity component of the sensor state vector must be determined if a six element state vector will be propagated over a few days.

Assuming the first ephemeris position data point is exact, the remainder of the position ephemeris can be fit using a least squares algorithm. The first difference is an excellent first guess to the velocity required to "hit" all of the remaining position ephemeris points. Once converged,

4

the sensor state vector will be the best possible estimate given the data at hand.

The next step is to refine the derived state vector from the Gauss algorithm using a least squares estimator. Assuming the Gauss-derived estimate is reasonable, the target vector can be improved up to the error of the data. The 1-$\sigma$ error figures of merit from the sensor specifications are used as an input into the program. These inputs form the data weighting matrix required by the least squares algorithm to normalize the data entries (see p. 37).

With the fastwalker orbit now defined, it can be propagated forward to determine the next encounter with another sensor in this or another constellation. This is easily done with the Air Force Jet Propulsion Laboratory's Long Term Orbit Predictor (LOP). The accuracy of this predictor has been proven with simulations matching probe flight and highly eccentric orbit trajectories.

## II.  Orbit Generation Equations and Methods

This chapter presents the equations necessary to accu-
rately model the motion of an orbiting object over short and
long periods of time.  This includes the differential equa-
tions of motion, transformation from an inertial state vector
to classical orbital elements.  Also included are the trans-
formation from the sensor coordinate system to the inertial
coordinate frame, which is the computational coordinate sys-
tem.  These transformations will be necessary for the weighted
least squares (also known as differential correction) process
where the observed measurements are compared to the assumed
or estimated measurements.

## Coordinate Systems and Transformations

Many different coordinate systems are quite useful for
expressing the orbit of an artificial satellite.  Two major
coordinate systems, the sensor coordinate frame and the iner-
tial coordinate frame will be described here.

The computational coordinate system for this algorithm,
the frame in which the equations of motion are expressed and
integrated, is the Earth Centered Inertial, or ECI coordinate
system shown in Figure 1, p. 7.  The origin of this frame is
at the center of the ellipsoidal earth model; the X-Y plane
is the equatorial plane of the earth and the Z-axis is coinci-

6

$$r = R + L\rho$$
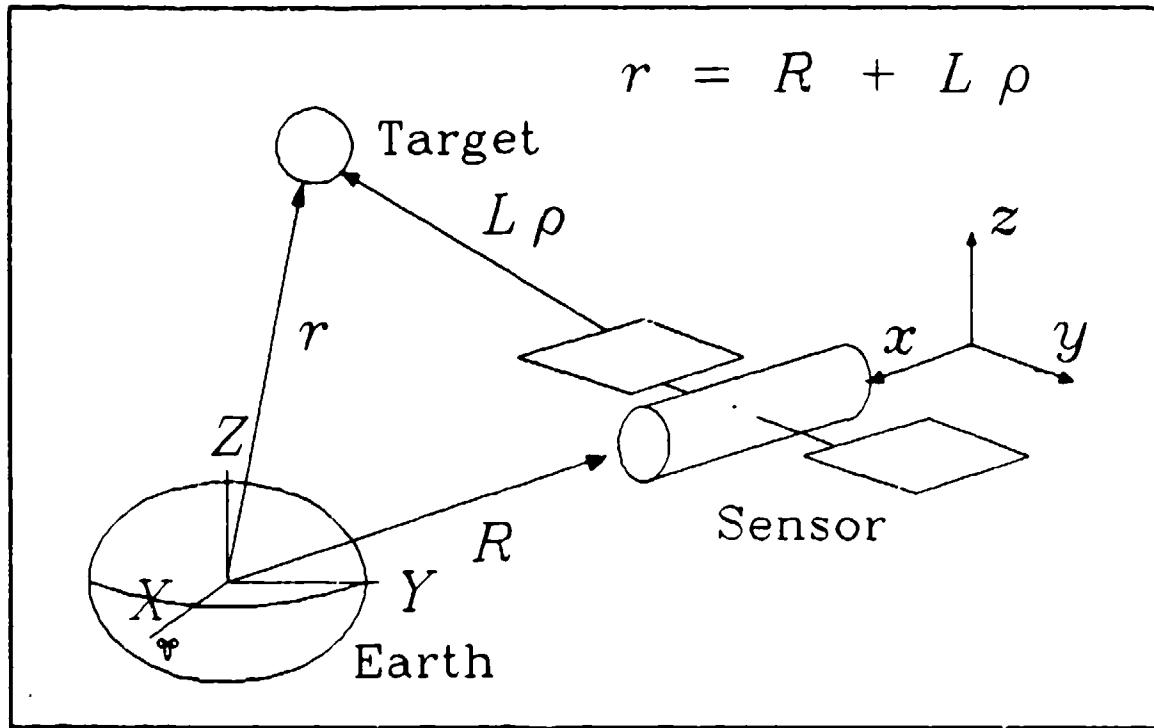
**Figure 1**     Fastwalker Problem Geometry

dent with the earth's axis of rotation.   This coordinate system is fixed in inertial space with X pointing toward the first point of Ares at some arbitrarily chosen time $t_0$.   For this program, $t_0$ is the midpoint of the data set for the initial estimate of the state vector and the time of the first data point for the WLS estimation process.

Two latitude types are normally associated with an ellipsoidal earth model -- the geocentric and geodetic latitudes (see Figure 2, p. 9).   The geocentric latitude is defined as the angle between the equatorial plane and the vector from

7

the center of the earth to the satellite subpoint. Geodetic latitude on the other hand is the angle between the equatorial plane and the line perpendicular to the subpoint tangent (local horizontal). The two are related by (1:97)

$$\tan \varphi^* = (a/b)^2 \tan \varphi \qquad (2.1)$$

where $\varphi$ is the geocentric latitude, $\varphi^*$ is the geodetic latitude and a and b are the earth's semimajor and semiminor axes respectively. Geocentric latitude is used for all computations. If the latitudes are input as geodetic, they are converted to geocentric.

The other coordinate system is the sensor-fixed system where the x-axis is pointing toward the origin of the ECI frame; the y-axis is parallel with the equatorial plane of the earth and the z-axis forms a right-handed coordinate system where x X y = z  (upper case letters denote the inertial frame, lower case letters denote sensor frame).

Within the sensor frame, the target is measured in azimuth and elevation. Azimuth is measured in the detector plane clockwise from "north"; elevation is measured up from the nadir (x-axis) direction (see Figure 3, p. 11). Both can be expressed in the ECI frame

$$\cos(El) = \frac{R_x\, \rho_x + R_y\, \rho_y + R_z\, \rho_z}{R\, \rho} \qquad (2.2)$$

8
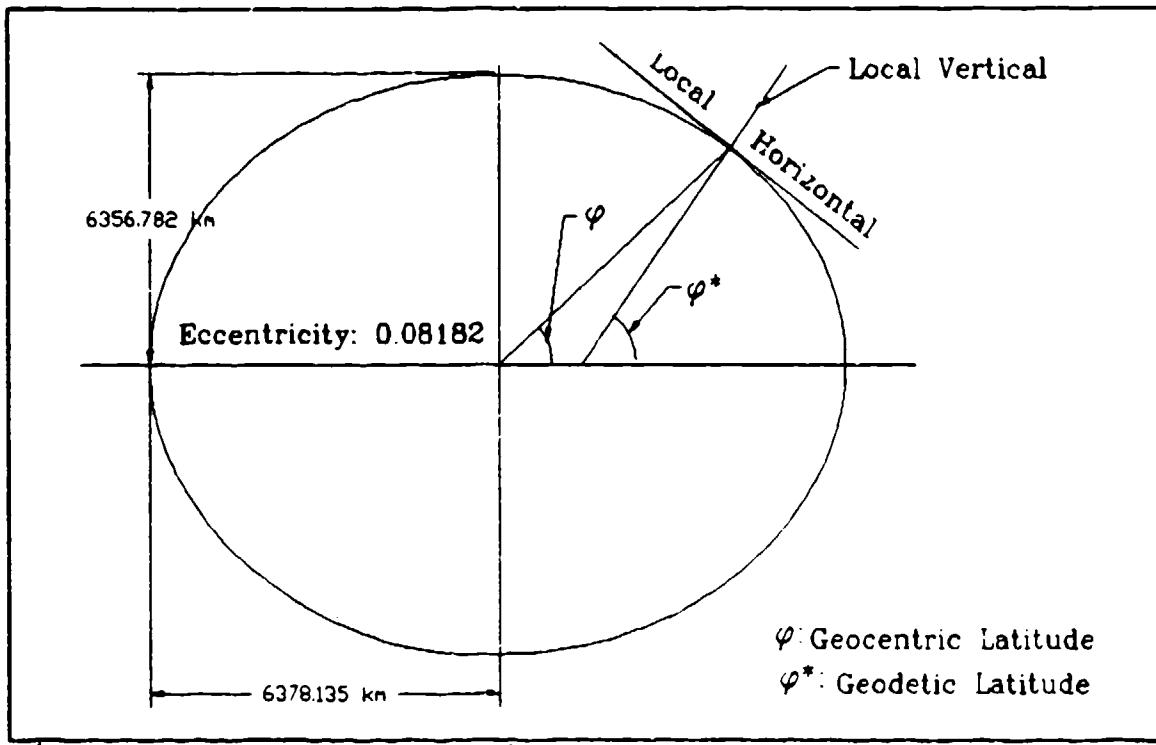
**Figure 2**          Ellipsoidal Earth Model

$$\tan (Az) = \frac{\sin A}{\cos A} \qquad (2.3)$$

$$\sin A = R \ (R_x \ \rho_y - R_y \ \rho_x) \qquad (2.4)$$

$$\cos A = \rho z \ (R_x^2 + R_y^2) - R_s \ (R_x \ \rho_x + R_y \ \rho_y) \qquad (2.5)$$

where $R_x$, $R_y$ and $R_s$ are the inertial sensor vector elements and $\rho_x$, $\rho_y$ and $\rho_s$ are the inertial slant range vector elements. Projecting the range unit vector upon the sensor coordinate frame produces the direction cosines $L_{xs}$, $L_{ys}$ and $L_{ss}$ where

$$L_{xs} = \cos az \qquad (2.6)$$

9
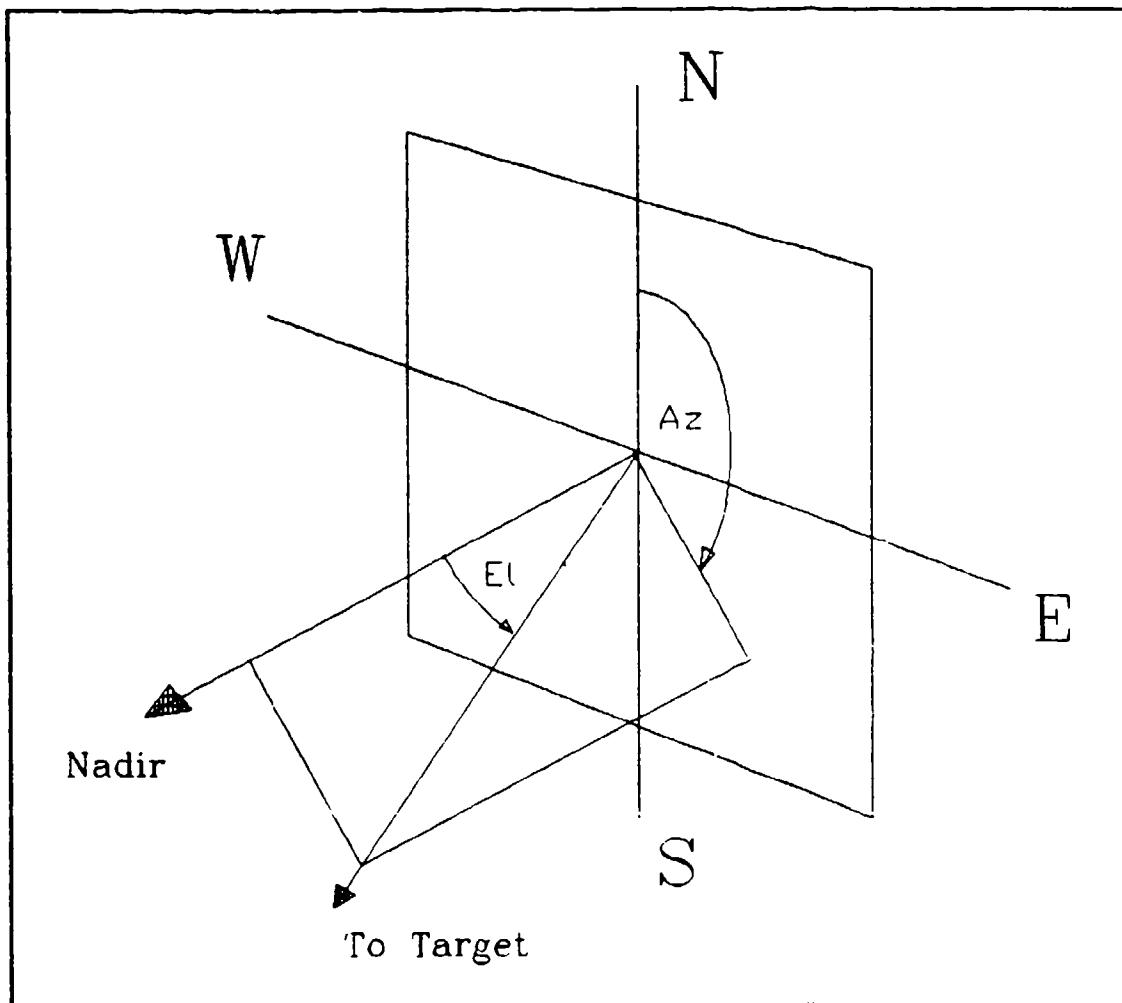
**Figure 3**          Fastwalker Sensor Geometry

$$L_{y_s} = -\sin el \sin az \qquad (2.7)$$

$$L_{z_s} = \sin el \cos az. \qquad (2.8)$$

A bias and scale factor is added to each azimuth and elevation
calculation to account for other metric data formats.

10

The two coordinate systems are related by two rotations.
The first rotation is about the sensor y-axis by the latitude
and then about the sensor z-axis by the local hour angle.
Mathematically,

$$
\begin{bmatrix} \rho_{xi} \\ \rho_{yi} \\ \rho_{zi} \end{bmatrix}
=
\begin{bmatrix}
\cos \alpha \cos \beta & \sin \alpha & -\cos \alpha \sin \beta \\
-\sin \alpha \cos \beta & \cos \alpha & \sin \alpha \sin \beta \\
\sin \beta & 0 & \cos \beta
\end{bmatrix}
\begin{bmatrix} \rho_{xs} \\ \rho_{ys} \\ \rho_{zs} \end{bmatrix}
\qquad (2.9)
$$

where

    $\rho_{xi}$, etc. = inertial frame slant range vector elements

    $\rho_{xs}$, etc. = sensor frame slant range vector elements

    $\alpha$ = -local hour angle = $-[\ \theta_{go} + \omega_e(t+t_o) + \lambda_s\ ]$

    $\theta_{go}$ = Greenwich hour angle at midnight

    $\omega_e$ = earth's rotation rate

    $t+t_o$ = time since midnight

    $\lambda_s$ = sensor longitude

    $\beta$ = $-\varphi_s$ = sensor latitude.

## Geopotential and Gravity Determination

Assuming a non-thrusting satellite above the earth's
atmosphere, the only significant force acting on the body over
a data span is gravity. Lillard in his thesis assumes negli-
gible longitude dependence, hence the earth's geopotential
becomes (16:18)

11

$$U = \mu/r \; [ \; 1 - \Sigma \; J_n \; (a_e/r)^n \; P_n(\sin(\varphi)) \; ], \qquad (2.10)$$

$\mu$ = Earth's gravitation constant 398600.8 km$^3$/sec$^2$

r = distance from center of the earth to the satellite

$J_n$ = harmonic constants

$a_e$ = earth's equatorial radius, 6378.135 km

$P_n$ = associated Legendre function

$\varphi$ = geocentric latitude.

This is also known as the zonal potential, which will be quite sufficient for the initial orbit estimate due to short data tracks relative to the time for perturbations to take effect. Hence four expansion terms are adequate. For long term propagation, tesseral and sectoral harmonics and other effects such as third body effects, solar drag, etc. must be included.

The acceleration due to gravity is derived from the above potential. Since $U$ is a solution to Laplace's equation, the gravity $g_o$ is simply the gradient of $U$, or

$$g_o = - \; \nabla \; (U). \qquad (2.11)$$

By setting

$$\sin(\varphi) = z/r$$

the geopotential and gravitational acceleration can be written entirely in the computational coordinate system, eliminating

12

the need to transform coordinates. Therefore, the gravitational acceleration becomes

$$X'' = -\frac{\mu X}{r^3} \left\{ 1 + J_2 \left[\frac{a_e}{r}\right]^2 \frac{3}{2} \left[1 - 5\frac{z^2}{r^2}\right] + J_3 \frac{z}{r} \left[\frac{a_e}{r}\right]^3 \frac{5}{2} \left[3 - 7\frac{z^2}{r^2}\right] \right.$$

$$\left. + J_4 \left[\frac{a_e}{r}\right]^4 \frac{5}{8} \left[-3 + 42\frac{z^2}{r^2} - 63\frac{z^4}{r^4}\right] \right\} \qquad (2.12)$$

$$Y'' = X''\frac{Y}{X} \qquad (2.13)$$

$$Z'' = -\frac{\mu Z}{r^3} \left\{ 1 + J_2 \left[\frac{a_e}{r}\right]^2 \frac{3}{2} \left[3 - 5\frac{z^2}{r^2}\right] + \right.$$

$$+ J_3 \left[\frac{a_e}{r}\right]^3 \frac{32}{2r} \left[-1 + 10\frac{z^2}{r^2} - \frac{35}{3}\frac{z^4}{r^4}\right] \right\}$$

$$\left. + J_4 \left[\frac{a_e}{r}\right]^4 \frac{5}{8} \left[-15 + 70\frac{z^2}{r^2} - 63\frac{z^4}{r^4}\right] \right\} \qquad (2.14)$$

where (") denotes the second derivative with respect to time. These equations of motion are integrated using a Runge-Kutta-Nystrom numerical integrator to propagate the state along in time.

13

## Orbital Element Generation

For this specific problem, Escobal states the Gaussian method of orbit determination is "second to none" when the time between the observations is small (6:272). The Laplace method was found to be unsuitable since the direction cosine rates and accelerations were small enough to produce near-singular matrices.

The Gauss method hinges on the fact that only two linearly independent vectors are needed to define the orbit plane, assuming negligible perturbation effects during the data span. Therefore a third vector can be written as a linear combination of the independent vectors. Thus it is possible to determine a set of constants a, b, and c not all zero such that

$$a r_1 + b r_2 + c r_3 = 0. \qquad (2.15)$$

Arbitrarily choosing $r_2$ as the dependent vector and redefining constants to $c_1$ and $c_2$

$$r_2 = c_1 r_1 + c_2 r_3. \qquad (2.16)$$

Crossing $r_2$ with $r_1$ and $r_3$ three parallel vectors perpendicular to the orbit plane are found whereby

$$r_1 \ X \ r_2 = r_1 r_2 \sin \nu_{12} = 2A_{12} W$$
$$r_2 \ X \ r_3 = r_2 r_3 \sin \nu_{23} = 2A_{23} W \qquad (2.17)$$
$$r_1 \ X \ r_3 = r_1 r_3 \sin \nu_{13} = 2A_{13} W$$

14

where $A_{ij}$ are the areas of the triangles formed by the respective radius vectors and $\nu_{ij}$ is the angle between the respective vectors.

Substituting,

$$A_{12}W = c_3 A_{13}W , \quad A_{23}W = c_1 A_{13}W$$

or

$$c_1 = \frac{A_{23}}{A_{13}} , \quad c_3 = \frac{A_{12}}{A_{13}} . \tag{2.18}$$

The Gauss method only requires observations at three different times. Since data sets of more than three observations are available, the set to be analyzed must be "averaged" in some sense (in this case, time). The number of data points was divided into three batches and the average time of each batch was used as the batch times. An $n^{th}$-order least squares polynomial (determined by the using analyst) is fit to each data coordinate to smooth through the noise. Then based upon the resulting equation, ECI direction cosines and sensor location for each batch time can be calculated and stored.

The above area ratios can be expressed as a function of time. For instance,

$$A_{12} = 1/2W \cdot [r_1 \ X \ r_2] \tag{2.19}$$

15

along with $r_1$ expressed in terms of $r_2$ in f and g series (see p. 28 for derivation), i.e.

$$r_1 = f_1 r_2 + g_1 r'_2 \qquad (2.20)$$

Substituting,

$$A_{12} = 1/2W \cdot [(f_1 r_2 + g_1 r'_2)] \times r_2] = -h g_1/2 \qquad (2.21)$$

where h is the orbital angular momentum. Similarly $A_{23}$ can be expressed as

$$A_{23} = 1/2W \cdot [(f_3 r_2 + g_3 r'_2)] \times r_2] = -h g_3/2 \qquad (2.22)$$

Note that there a common area $A_{13}$, where

$$A_{13} = 1/2W \cdot [(f_1 r_2 + g_1 r'_2)] \times (f_3 r_2 + g_3 r'_2)] \qquad (2.23)$$

or

$$A_{13} = 1/2h \ (f_1 g_3 - f_3 g_1) \qquad (2.24)$$

In terms of the f and g expansions, the coefficients $c_1$ and $c_3$ are

$$c_1 = \frac{g_3}{f_1 g_3 - f_3 g_1}$$

$$\qquad (2.25)$$

$$c_3 = \frac{g_1}{f_1 g_3 - f_3 g_1}$$

16

Truncating the f and g series after the second term, $c_1$ and $c_3$ can be approximated by

$$c_1 \approx \frac{\tau_3}{\tau_{13}} \left\{ 1 + \frac{u_2}{6} (\tau_{13}{}^2 - \tau_3{}^2) \right\}$$

$$c_3 \approx -\frac{\tau_1}{\tau_{13}} \left\{ 1 + \frac{u_2}{6} (\tau_{13}{}^2 - \tau_1{}^2) \right\}$$

(2.26)

where $u_2 = \mu/r^2$. By allowing

$$A_1 = \frac{\tau_3}{\tau_{13}} \qquad\qquad B_1 = \frac{\tau_3}{6\tau_{13}} (\tau_{13}{}^2 - \tau_3{}^2)$$

$$A_3 = -\frac{\tau_1}{\tau_{13}} \qquad\qquad B_3 = -\frac{\tau_1}{6\tau_{13}} (\tau_{13}{}^2 - \tau_1{}^2),$$

$c_1 \approx A_1 + B_1 u_2$ and $c_3 \approx A_3 + B_3 u_2$, where $c_2 = -1$.

The vector equation $r_2 = c_1 r_1 + c_3 r_3$ can be modified using the basic relation $r = \rho - R$ to produce the equation

$$c_1 \rho_1 + c_2 \rho_2 + c_3 \rho_3 = c_1 R_1 + c_2 R_2 + c_3 R_3.$$

The vector $\rho_1$ can be written as a product of the direction cosine matrix $L$ and magnitude $\rho$. The resulting equation takes the form

$$c_1 \rho_1 L_1 + c_2 \rho_2 L_2 + c_3 \rho_3 L_3 = G$$

(2.27)

17

where $G = c_1 R_1 + c_2 R_2 + c_3 R_3$. Thus the previous equation can be expressed in matrix form as

$$
\begin{bmatrix}
L_{x1} & L_{x2} & L_{x3} \\
L_{y1} & L_{y2} & L_{y3} \\
L_{z1} & L_{z2} & L_{z3}
\end{bmatrix}
\begin{bmatrix}
c_1 \rho_1 \\
c_2 \rho_2 \\
c_3 \rho_3
\end{bmatrix}
=
\begin{bmatrix}
G_x \\
G_y \\
G_z
\end{bmatrix}
\qquad (2.28)
$$

It is possible to form the inverse of the matrix $L$, solving for the $c_i \rho_i$ matrix. If $a_{ij}$ denotes the individual elements of $L^{-1}$ and vectors

$$A = [A_1, -1, A_3]^T \ , \ B = [B_1, 0, B_3]^T \ , \ X = [X_1, X_2, X_3]^T \ ,$$

$$Y = [Y_1, Y_2, Y_3]^T \ , \ \text{and} \ Z = [Z_1, Z_2, Z_3]^T$$

then the slant range $\rho_i$ for each batch time is

$$
\rho_1 = \frac{A_1^* + B_1^* u_2}{A_1 + B_1 u_2}
$$

$$
\rho_2 = A_2^* + B_2^* u^2 \qquad (2.29)
$$

$$
\rho_3 = \frac{A_3^* + B_3^* u_2}{A_3 + B_3 u_2}
$$

where

$$A_1^* = (a_{11} A \cdot X + a_{12} A \cdot Y + a_{13} A \cdot Z)$$

$$B_1^* = (a_{11} B \cdot X + a_{12} B \cdot Y + a_{13} B \cdot Z)$$

$$A_2^* = -(a_{21} A \cdot X + a_{22} A \cdot Y + a_{23} A \cdot Z)$$

$$B_2^* = -(a_{21} B \cdot X + a_{22} B \cdot Y + a_{23} B \cdot Z)$$

$$A_3^* = (a_{31} A \cdot X + a_{32} A \cdot Y + a_{33} A \cdot Z)$$

18

$$B_3' = (a_{31}B'X + a_{32}B'Y + a_{33}B'Z).$$

To determine the magnitude of the target's radius vector another equation is required. Another linearly independent relation can be derived by dotting the vector equation relating target position to sensor position into itself, producing

$$r_2^2 = \rho_2^2 - 2\rho L_2 \cdot R_2 + R_2^2. \tag{2.30}$$

The scalar products $L \cdot R$ are known from the collected angular observations and sensor location. At the center batch time $t_2$, let

$$C_2 = -2(X_2 L_{x2} + Y_2 L_{y2} + Z_2 L_{z2}).$$

Substituting $\rho_2$ and $C_2$ into the resultant dot product equation

$$r_2^8 - (C_2 A_2' + A_2'^2 + R_2^2) r_2^6 - \mu(C_2 B_2' + 2A_2' B_2') r_2^3)$$
$$- \mu^2 B_2'^2 = 0. \tag{2.31}$$

One is not assured of a real root since this equation is of even order. By factoring this equation, all possible combinations of reasonable roots can be explored by the analyst. The classical Newton-Raphson root finding technique finds only one root based upon an initial guess. Hence the former method was chosen.

Velocity is found by first taking a Taylor series expansion of $r_2$, i.e.,

19

$$r_j = \sum_{i=1}^{\infty} \frac{(\tau_{ij})^i}{i!} \, r_2^{(i)}, \quad j=1,3 \tag{2.32}$$

where $\tau_{ij} = (\tau_j - \tau_i)$, $\tau_i$ being the epoch time. When the expansion is written for batch times 1 and 3, time 2 being epoch

$$r_1 - r_2 = -\tau_{12}r_2' + \tau_{12}^2 \frac{r_2''}{2} - \tau_{12}^3 \frac{r_2'''}{6} + \tau_{12}^4 \frac{r^{IV}}{24} + O(\tau_{12}^5) \tag{2.33}$$

$$r_3 - r_2 = \tau_{23}r_2' + \tau_{23}^2 \frac{r_2''}{2} + \tau_{23}^3 \frac{r_2'''}{6} + \tau_{23}^4 \frac{r^{IV}}{24} + O(\tau_{23}^5) \tag{2.34}$$

Multiplying equation (2.33) by $\tau_{23}$, equation (2.34) by $\tau_{12}$ and adding produces an equation void of $r_2'$. Now multiplying the equation (2.33) by $-\tau_{23}^2$ and equation (2.34) by $\tau_{12}^2$ and adding produces an equation void of $r_2''$. Differentiating each of these new expressions yields

$$\tau_{12}r_1 - \tau_{23}r_2'' + \tau_{12}r_3'' = \tau_{12}\tau_{23}\tau_{13} \, 1/2 \, r_2^{IV} + O(r_2^V) \tag{2.35}$$

$$-\tau_{23}^2 r_1'' + (\tau_{23}^2 - \tau_{12}^2)r_2'' + \tau_{12}^2 r_3'' = \tau_{12}\tau_{23}\tau_{13} \, r_2''' +$$
$$O(r_2^{IV}). \tag{2.36}$$

Assuming the $O(r^{IV})$ terms can be ignored, one can solve for $r_2^{IV}$ and $r_2''$ and substituting the respective derivatives into the equation void of $r_2''$ derived above generates

20

$$\tau_{12}\tau_{23}\tau_{13} \; \mathbf{r}_2' = -\tau_{23}{}^2\mathbf{r}_1 + (\tau_{23}{}^2 - \tau_{12}{}^2)\mathbf{r}_2'' + \tau_{12}{}^2\mathbf{r}_3'' -$$

$$\frac{\tau_{12}\tau_{23}\tau_{13}}{12} \; [ \; -\tau_{23}{}^2\mathbf{r}_1'' + (\tau_{23}{}^2 - \tau_{12}{}^2)\mathbf{r}_2'' + \tau_{12}{}^2\mathbf{r}_3'' \; ]. \quad (2.37)$$

Substituting the two-body equation of motion into the second derivative terms and allowing

$$H_1 = \frac{\mu\tau_3}{12} \qquad\qquad G_1 = -\frac{\tau_3}{\tau_1\tau_{13}}$$

$$H_3 = -\frac{\mu\tau_1}{12} \qquad\qquad G_3 = -\frac{\tau_1}{\tau_3\tau_{13}}$$

$$H_2 = H_1 - H_3 \qquad\qquad G_2 = G_1 - G_3$$

then

$$d_i = G_i + \frac{H_i}{r_i{}^3} \; , \quad i=1,2,3 \qquad\qquad (2.38)$$

and

$$\mathbf{v} = -d_1\mathbf{r}_1 + d_2\mathbf{r}_2 + d_3\mathbf{r}_3. \qquad\qquad (2.39)$$

At this point, the orbit is considered determined since both $r$ and $v$ are known.

21

## Orbital Element Sets

Orbital elements are sets of six or more parameters which describe an orbit, whether be in size, shape, orientation, energy, momentum, etc. Of the three main types -- classical, equinoctial, and Delaunay -- the equinoctial element set provides the best accuracy since there are no singularities as there are in the classical and Delaunay sets, except at i=180°. The drawback, however, is that the equinoctial set is rather abstract compared to the classical set.

The equinoctial elements in terms of the classical element set for a direct orbit are:

$$a = a \qquad\qquad \lambda = M_0 + \omega + \Omega$$

$$h = e \sin (\omega + \Omega) \qquad k = e \cos (\omega + \Omega) \qquad (2.40)$$

$$p = \tan (i/2) \sin \Omega \qquad q = \tan (i/2) \cos \Omega.$$

Deriving these elements in terms of the state vector requires a little more knowledge of the geometry involved. Cefola in Figure 4 (p. 23) shows graphically what the equinoctial set represents (4:2). The orientation of the coordinate system is defined by an angle equal to the longitude of the ascending node, $\Omega$, and the unit vector w perpendicular to the orbit plane. Unit vector f is in the orbit plane specified by i/2 down from Ares and an angle $\Omega$ down from the node. Vector g forms the right-handed triad such that f X g = w.

22
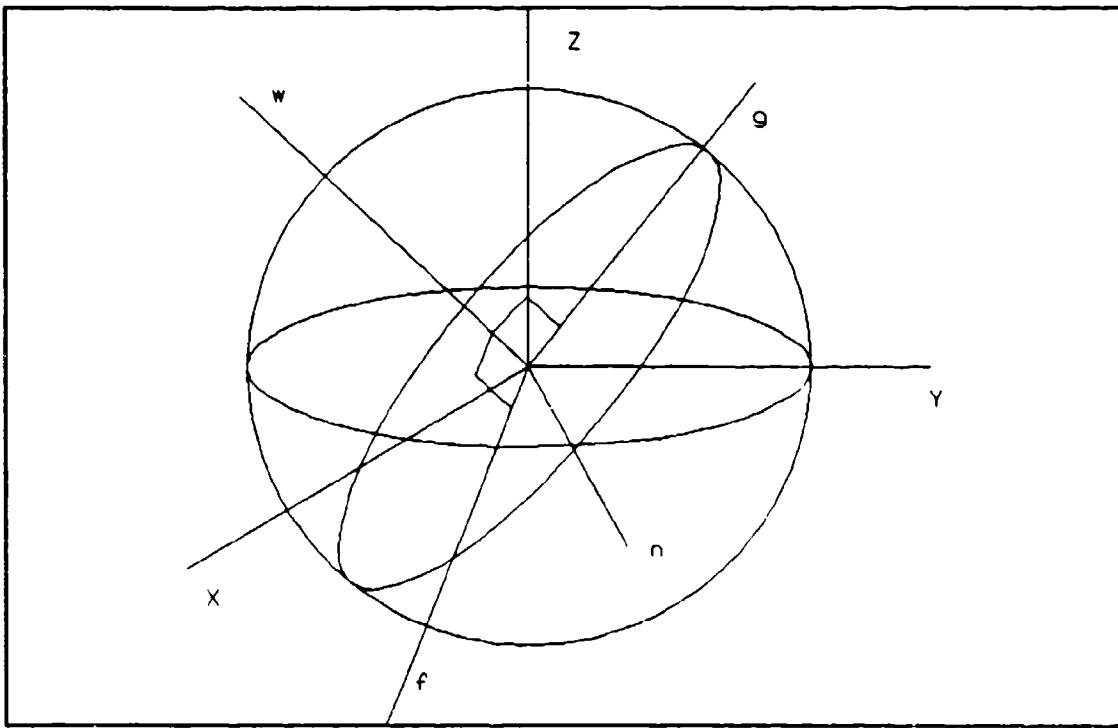
**Figure 4**          Equinoctial Coordinate Frame

An orbit's shape is defined by the elements h and k, which are the components of the eccentricity vector projected upon the **f** and **g** vectors.  The element $\lambda_0$ pinpoints the position of the satellite on the orbit since it is the sum of the three angles measured in the plane.  The final two elements, p and q, are the most abstract.  In short, these elements merely characterize the orientation of the orbit.  Both are required in the rotation matrix to transform the inertial frame to the equinoctial frame (4:3).

23

For the direct orbit case, the unit vectors can be mathematically expressed as

$$f = \frac{1}{1 + p^2 + q^2} \left\{ \begin{array}{c} 1 - p^2 + q^2 \\ 2pq \\ -2p \end{array} \right\} \qquad (2.41)$$

$$g = \frac{1}{1 + p^2 + q^2} \left\{ \begin{array}{c} 2pq \\ 1 + p^2 - q^2 \\ 2q \end{array} \right\} \qquad (2.42)$$

$$w = \frac{1}{1 + p^2 + q^2} \left\{ \begin{array}{c} 2p \\ -2q \\ 1 - p^2 - q^2 \end{array} \right\} \qquad (2.43)$$

## Transformation from an ECI State Vector to Equinoctial Elements

The transformation from the state vector to the equinoctial elements is a fairly straight forward once the coordinate frame is understood. An orbit's specific energy directly produces the semimajor axis since

$$a = - \frac{\mu}{2} \left[ \frac{v^2}{2} - \frac{\mu}{r} \right]^{-1} . \qquad (2.44)$$

The eccentricity vector is given by

$$e = \frac{1}{\mu} \left\{ \left[ v^2 - \frac{\mu}{r} \right] r - (r \cdot v) v \right\} \qquad (2.45)$$

24

Another way to express the unit normal to the orbit plane is through the angular momentum, r X v.  Hence

$$\mathbf{w} = \frac{r \ X \ v}{|r \ X \ v|} .$$

(2.46)

However, this expression has the same exact meaning as the previous w equation in terms of p and q.  Therefore, p and q are

$$p = \frac{\mathbf{w}_x}{1 + \mathbf{w}_z} \qquad q = - \frac{\mathbf{w}_y}{1 + \mathbf{w}_z}$$

(2.47)

and the equinoctial elements h and k are merely

$$h = e \cdot g , \quad k = e \cdot f.$$

(2.48)

The remaining element to derive is the mean longitude, $\lambda_0$.  First compute the position coordinates X and Y relative to the orbital frame f-g-w by

$$X = x \cdot f, \quad Y = x \cdot g.$$

(2.49)

Then compute

$$\cos F = k + \frac{(1 - k^2\beta)X - hk\beta Y}{a(1 - h^2 - k^2)^{1/2}}$$

(2.50)

$$\sin F = h + \frac{(1 - k^2\beta)Y - hk\beta X}{a(1 - h^2 - k^2)^{1/2}}$$

25

where the variable β is

$$\beta = \frac{1}{1 + (1 - h^2 - k^2)^{1/2}}.$$

Then the mean longitude is given by

$$\lambda_0 = F - k \sin F + h \cos F. \qquad (2.51)$$

These equations are mainly used to compute the numerical partials for the Jacobian transforming the ECI state vector covariance matrix to the equinoctial element covariance matrix.

26

# III.  Propagation Methods

In order to calculate the sensor and target state vectors at times other than the epoch, the state must be propagated via some numerical technique.  There are various methods to propagate the state along in time so that the calculated measurements can be compared to the actual observations.  For this thesis, however, three main methods are used, each having a particular purpose.  Two methods are used to propagate the state -- the $4^{th}$-Order Runge-Kutta-Nystrom numerical integrator and f and g series expansions.  A state transition matrix is used to propagate the covariance matrix, which consists of partial derivatives of the present state with respect to the estimated epoch state.  The covariance matrix will be examined in the next chapter.  Each propagation method will be briefly described.

## 4th Order Runge-Kutta-Nystrom (RKN) Numerical Integrator

The RKN integrator is a closed form predictor-corrector numerical integrator specifically suited for $2_{nd}$ order differential equations.  One of the novelties of this integrator is that the position and velocity at time t+$\Delta$t are direct outputs, so only one integration pass is required per time step.

Battin does an excellent job of deriving the RKN integrator in minute detail (2:577).  However, Kreysig describes

27

the method in terms of a scalar function which is easier to follow (15:1078).

The RKN numerical integrator algorithm is

$$x = x_0 + hy_0 + h^2(k_0 + 2k_1)/6 + O(h^5)$$
$$y = y_0 + h(k_0 + 4k_1 + k_2)/6 + O(h^5)$$

(3.1)

where

$$k_0 = f(t_0, x_0)$$
$$k_1 = f(t_0 + h/2, x_0 + hy_0/2, h^2 k_0/8)$$
$$k_2 = f(t_0 + h, x_0 + hy_0, h^2 k_1/2) \quad .$$

This algorithm is best suited for accurate propagation of a state vector in an estimation routine since a precise state estimate is required at each data point. In addition, other effects can be included in the function $f(t,x,y)$ to exactly model the physics of the problem.

## F and G Series

The f and g series expansions are series solutions of the two-body equation of motion. In other words, any position r can be expressed in terms of the epoch position $r_0$ and the time $\tau$ from the epoch to the time desired. Mathematically, any function can be expressed as an infinite series, i.e.

$$r = \sum \frac{\tau^n}{n!} \, r^{(n)} \tag{3.2}$$

which is the form of a Taylor Series about zero (also known as a MacLaurin Series.)

Assuming that the above series is a solution, differentiate the two-body equation of motion three times (making this expansion of fifth-order) holding the epoch time $t_0$ constant and substituting $r_0'' = ur_0$ ($u=\mu/r^3$) wherever $r_0''$ appears. The resulting equations are

$$r_0^{III} = -u'r_0 - ur_0'$$
$$r_0^{IV} = (-u'' + u^2)r_0 - 2u'r_0' \tag{3.3}$$
$$r_0^{V} = (-u^{III} + 4uu')r_0 - (3u'' - u^2)r_0'.$$

Substituting these expressions into the Taylor series produces the familiar equation

$$r = fr_0 + gr_0', \tag{3.4}$$

where

$$f = 1 - 1/2 \, u\tau^2 - 1/6 \, u'\tau^3 - 1/24 \, (u'' - u^2)\tau^4 - 1/120(u^{III}$$
$$- 4uu')\tau^5 \tag{3.5a}$$

and

$$g = \tau - 1/6 \, u\tau^3 - 1/12 \, u'\tau^4 - 1/120(3u'' - u^2)\tau^5. \tag{3.5b}$$

29

In this form the f and g expressions are useless from a practical point of view since higher order derivatives of u are not known. Escobal states Lagrange proceeds as follows (6:109). Introduce the new variables p and q such that

$$r^2 p = \frac{d(r^2)}{d\tau} \quad , \quad r^2 q = \frac{d^2(r^2)}{d\tau^2} \qquad (3.6)$$

where

$$p \equiv \frac{rr'}{r^2} = \frac{\mathbf{r} \cdot \mathbf{r'}}{r^2} \quad , \quad q \equiv \frac{r'^2 - r^2 u}{r^2} \; .$$

so,

$$u' = -\frac{3\mu}{r^4} \frac{dr}{d\tau} = -\frac{3\mu}{2r^5} \frac{d(r^2)}{d\tau}$$

$$p' = \frac{1}{2r^2} \frac{d^2(r^2)}{d\tau^2} - \frac{1}{r^3} \frac{d(r^2)}{d\tau} \frac{dr}{d\tau} \qquad (3.7)$$

$$q' = -\frac{1}{r^3} \frac{d^2(r^2)}{d\tau^2} \frac{dr}{d\tau} + \frac{1}{r^3} \frac{d^3(r^2)}{d\tau^3}$$

which become by introduction of the previously defined p and q

$$u' = -3up$$
$$p' = q - p^2 \qquad (3.8)$$
$$q' = -(up + 2pq).$$

30

Differentiating u',

$$u'' = -3(up' + u'p),$$

which becomes

$$u'' = -3[u(q - 2p^2) - 3up^2] \qquad (3.9)$$

via substituting p and q. This process can be repeated to eliminate u', p' and q' from each derivative. Therefore, the 5$^{th}$ order f and g series expansions are

$$f = 1 - 1/2\ u\tau^2 + 1/2\ up\tau^3 + 1/24\ (3uq - 15up^2 + u^2)\tau^4 +$$
$$1/8\ (7up^3 - 3upq - u^2p)\tau^5 \qquad (3.10)$$

$$g = \tau - 1/6\ u\tau^3 + 1/4\ up\tau^4 + 1/120\ (9uq - 45up^2 + u^2)\tau^5. \qquad (3.11)$$

These expressions are used to obtain a quick initial state estimate at the beginning of the data track. Since the series is truncated at $O(\tau^4)$, this method is definitely not suited for long term propagation. As long as the initial target state estimate is "good", the least squares estimator can properly refine it.

31

## State Transition Matrix

In order to create the partial derivative matrix required for the least squares process, the partial derivatives of $Az_i$ and $El_i$ must be taken with respect to the state vector at the epoch time. Partial derivatives of the $i^{th}$ data point can be related to the epoch state vector by the state transition matrix, $\Phi(t_{i+1}, t_i)$. This matrix is derived in many control theory texts, but its use for our purposes Wiesel derives it in terms of the required dynamical equations (18:26). In short, the state transition matrix demonstrates how the state changes in time but in matrix format.

The state transition matrix is derived from the solution of the matrix differential equation

$$\frac{d}{dt} \Phi(t, t_o) = A(t) \; \Phi(t, t_o) \qquad (3.12)$$

where in this case $\Phi$ is more appropriately called the equations of variation since it contains the effects of all trajectories near the reference trajectory. In other words, it is not linearized. If one assumes that the changes in each element is negligible, $\Phi$ is a constant matrix. The matrix also takes on some interesting properties:

$$\Phi(t, t) = I \qquad (3.13a)$$

$$\Phi(t_2, t_o) = \Phi(t_2, t_1) \; \Phi(t_1, t_o) \qquad (3.13b)$$

$$\Phi(t, t_o) = \Phi(t_o, t)^{-1}. \qquad (3.13c)$$

32

The partial derivative matrix of the data with respect to the state vector at $t_i$ can be related to the epoch state vector $x_o$ by the chain rule (equation 3.13b). Let $H_i$ be the partial derivative comparing the changes in the data to the state elements at time $t_i$. Then $H_i$ is related to the epoch vector by

$$H_{i/o} = H_i \ \Phi(t_i, t_{i-1}) \ \Phi(t_{i-1}, t_{i-2}) \ \dots \ \Phi(t_2, t_1) \ \Phi(t_1, t_o) \quad (3.14)$$

where $H_{i/o}$ is the partial derivative matrix of the data at time $t_i$ with respect to the epoch state vector $x_o$ which is required for use in the least squares estimator.

# IV.  Refining the Initial State Estimate

The main method of refining the state vector derived from the Gauss orbit method is least squares.  The method of least squares, developed by Gauss for his astronomical studies in 1795, is concerned with estimating the values of a set of parameters of a measurement model, which relates the measurements to the parameters to be estimated (16:35).  These estimated measurements are then compared to a set observations to produce residuals.  The sum-squared residuals are minimized. The set of estimates which produces this minimum is said to be optimal in a least-squares sense (i.e. the azimuth and elevation data are the observations).  The initial state estimate produces a corresponding set of observations which are subtracted from the measured observations to produce residuals.

The parameters to estimate are called the state variables at some fixed time $t_o$ known as the epoch time.  If we let the vector $z_i$ represent the set of measured azimuth and elevation at time $t_i$, the observation model may be represented as

$$z = G_i(x_o, t_o) + \epsilon_i \ , \ i = 1, 2, \ldots, n \qquad (4.1)$$

where

    $n$ = total number of measurement times

    $x_o$ = the initial estimate of the state vector at epoch

$G_i$ = the vector of functions relating the state vector to the observations

$\epsilon_i$ = the error vector of the observations at time $t_i$.

Therefore, the observations can be notationally expressed as

$$Az_{m\,i} = Az_i + \epsilon_{A\,i}$$
$$El_{m\,i} = El_i + \epsilon_{E\,i}$$

(4.2)

where

$\epsilon_{A\,i}$, $\epsilon_{E\,i}$ = the $i^{th}$ azimuth and elevation measurement error

$Az_{m\,i}$, $El_{m\,i}$ = the $i^{th}$ measured azimuth and elevation

$Az_i$ and $El_i$ = the true azimuth and elevation at time $t_i$.

The minimum state vector for an orbiting object is the six-element vector

$$X_o = (X_o,\ Y_o,\ Z_o,\ X_o',\ Y_o',\ Z_o')$$

(4.3)

assuming a high altitude non-perturbed satellite. Perturbations, thrusting and other effects add extra elements. Since one of the assumptions is the object is non-thrusting and the data track is small with respect the time it takes for perturbations to take effect, these elements are ignored.

If the observation relations were linear, one could take any $n$ of them and solve for the unknown parameters, where m is the number of unknown state elements in the relations.

35

However, the observation relations are non-linear which forces us to expand the relations in an infinite series, truncate and then iterate. This is also known as linearization.

A perfect sensor would measure the perfect state $x_o$ producing the exact set of measurements $z_o$. Then the estimated state can be represented as $x = x_o + \delta x$. Hence the error vector $\epsilon$ is given by

$$\epsilon = z - z_o = G(x_o + \delta x) - H(x_o)$$

$$\approx \frac{\partial G}{\partial x} \delta x \qquad (4.4)$$

Let $\hat{x}_o$ be the estimate of $x_o$. Then the first-order approximation of the error by expanding the observation relations in a Taylor series is

$$\epsilon_{Az\ i} = Az_{ob\ i} - Az_i - \frac{\partial Az_i}{\partial x_o} \Delta x + O(\Delta x^2) \qquad (4.5)$$

$$\epsilon_{El\ i} = El_{ob\ i} - El_i - \frac{\partial El_i}{\partial x_o} \Delta x + O(\Delta x^2) \qquad (4.6)$$

where $\Delta x$ is the difference between the initial state and the state estimate. Then the partial derivative matrix of the observation relation G to the state elements is

36

$$\frac{\partial G}{\partial x} = \left\{ \begin{array}{cccccc} \dfrac{\partial Az_i}{\partial x_o} & \dfrac{\partial Az_i}{\partial y_o} & \dfrac{\partial Az_i}{\partial z_o} & 0 & 0 & 0 \\[3mm] \dfrac{\partial El_i}{\partial x_o} & \dfrac{\partial El_i}{\partial y_o} & \dfrac{\partial El_i}{\partial z_o} & 0 & 0 & 0 \end{array} \right\} \tag{4.7}$$

When the higher order terms are ignored, the Taylor series expansion produces a linear set of equations in $\Delta x$. Now we can apply the concept of non-linear least squares.

Let $\epsilon$ be the 2n X 1 matrix of error elements azimuth and elevation for each observation time

$$\epsilon = \{ \ \epsilon_{Az\ 1}, \ \epsilon_{El\ 1}, \ \epsilon_{Az\ 2}, \ \epsilon_{El\ 2}, \ \ldots, \ \epsilon_{Az\ n}, \ \epsilon_{El\ n} \ \}^T \tag{4.8}$$

$$H = \left\{ \ \frac{\partial G_1}{\partial x_o} \quad \frac{\partial G_2}{\partial x_o} \quad \frac{\partial G_3}{\partial x_o} \ \ldots \ \frac{\partial G_n}{\partial x_o} \right\}^T \tag{4.9}$$

$$b = \left\{ \begin{array}{l} Az_{ob\ 1} - Az_1(x,t_o) \\ El_{ob\ 1} - El_1(x,t_o) \\ Az_{ob\ 2} - Az_2(x,t_o) \\ El_{ob\ 2} - El_2(x,t_o) \\ \quad \cdot \\ \quad \cdot \\ Az_{ob\ i} - Az_i(x,t_o) \\ El_{ob\ i} - El_i(x,t_o) \end{array} \right\} \tag{4.10}$$

With the above matrix definitions, the linearized observation relations can be rewritten as

$$\epsilon = b - H\Delta x. \tag{4.11}$$

37

There are two types of residuals -- azimuth and elevation. Elevation is normally more accurate than azimuth, so the least squares process will try "fit" azimuth before it considers fitting elevation. Therefore weights must be applied to the data to normalize the residuals (7:48). This way the least squares process will consider each observation equally. Also weighting gives us the opportunity to ignore unwanted or erroneous data.

Assuming that the data is corrupted by Gaussian white noise (each observation is uncorrellated in time and space with zero mean), the weighting matrix $W$ is a diagonal matrix with the weightings on the diagonal. This is not true since a sensor takes raw measurements and then transforms them into something which can be understood. Also, if the observations are measured by a moving sensor they are correlated in time. However, these effects are generally small and the assumption is justified (5:B-3).

It is clear when weighting is introduced, the estimate will be a direct function of the weights. Lillard states the optimal weighting matrix is the inverse covariance matrix of the measurement errors (16:43). Considering the above assumptions, the weighting matrix is composed of error variances on the diagonal with the variances of each observation data type being equal.

Introducing the 2n X 2n weighting matrix $W^{1/2}$, the matrix error equation is

$$\epsilon_v = W^{1/2}b - W^{1/2}H\Delta x \qquad (4.12)$$

where the w subscript indicates the weighted error equation. "Squaring" $\epsilon$ produces the squared residual matrix

$$\epsilon_v^T\epsilon_v = (W^{1/2}b - W^{1/2}H\Delta x)^T (W^{1/2}b - W^{1/2}H\Delta x) \quad (4.13)$$

Now taking the partial derivatives with respect to $\Delta x$ and since we are looking for a minimum, setting it equal to zero gives the standard weighted least squares difference equation

$$\Delta x = (H^T W H)^{-1} H^T W b$$

$$(4.14)$$

$$P = (H^T W H)^{-1}.$$

with $P$ being the covariance matrix associated with the estimate where the diagonal terms are the variances and the off-diagonal terms are the covariances.

This equation is called a "difference" equation because it provides an update to the previous state estimate since the observation equations are non-linear. If they were linear there would be no need to iterate and the optimal least squares estimate is just $\Delta x + x_o$. Nonetheless, the optimal estimate for the non-linear case is found by continually

39

updating the state estimate until some convergence criteria
is reached.

Statistically,

$$\mathbf{P_x} = E(\delta\mathbf{x}\ \delta\mathbf{x}^{\tau}), \tag{4.15}$$

where $E$ is the expectation operator. Since the Taylor series
was truncated to first order,

$$\delta\mathbf{x} = \mathbf{J}\ \delta\mathbf{y}, \tag{4.16}$$

where $\mathbf{J}$ is the Jacobian of $\mathbf{x}$ with respect to $\mathbf{y}$. Substitut-
ing,

$$\mathbf{P_x} = E[\mathbf{J}\ \delta\mathbf{y}\ (\mathbf{J}\ \delta\mathbf{y})^{\tau}]$$

$$\mathbf{P_x} = E(\mathbf{J}\ \delta\mathbf{y}\ \delta\mathbf{y}^{\tau}\ \mathbf{J}^{\tau}). \tag{4.17}$$

Since $\mathbf{J}$ is a constant matrix, it can be brought outside of
the expectation operator producing

$$\mathbf{P_x} = \mathbf{J}\ E(\ \delta\mathbf{y}\ \delta\mathbf{y}^{\tau}\ )\ \mathbf{J}^{\tau}.$$

$$\mathbf{P_x} = \mathbf{J}\ \mathbf{P_y}\ \mathbf{J}^{\tau}. \tag{4.18}$$

Solving for $\mathbf{P_y}$,

$$\mathbf{P_y} = \mathbf{J}^{-1}\ \mathbf{P_x}\ (\mathbf{J}^{\tau})^{-1}. \tag{4.19}$$

Since $\mathbf{J}$ is an orthogonal symmetric matrix, $\mathbf{J}^{\tau} \equiv \mathbf{J}^{-1}$,

$$\mathbf{P_y} = \mathbf{J}^{\tau}\ \mathbf{P_x}\ (\mathbf{J}). \tag{4.20}$$

40

Therefore, given the functional relationship between x and y, any covariance matrix in one space can be transformed into another space via the above association.

## Unobservability

One of the main problems with least squares is that the initial estimate must be sufficiently "close" to a solution to ensure convergence. This is due to the fact that the Taylor series was expanded about a reference orbit and truncated beyond the linear term. The Gauss orbit determination method produces the initial state estimate for input into the least squares estimator. This estimate is a three dimensional estimate, however the data being fit is two-dimensional. In other words, one can determine the direction to the target with respect to the sensor, but the data contains no range information. Thus there will be an unobservable eigenvector parallel to the slant range vector corresponding to an infinite eigenvalue for $\mathbf{P}$.

In order for an estimate to exist, the matrix $\mathbf{H}^\tau \mathbf{W} \mathbf{H}$ must be invertible. This is called the observability condition (19:58). For our case, the zero eigenvalue of $\mathbf{P}^{-1}$ prevents inversion of this matrix to form the covariance but since computers introduce roundoff and other errors we can invert this ill-conditioned matrix. If this matrix is used

41

to find the state estimate the solution will rapidly diverge due to an uncontrollable $\Delta x$. To control $\Delta x$, decompose $P^{-1}$ into its eigenvalues and determine the contribution of the unobservable eigenvector into the state update.

Let $T$ be the matrix of eigenvectors of $P^{-1}$, so

$$T = ( \; \xi_1 \quad \xi_2 \quad \xi_3 \quad \xi_4 \quad \xi_5 \quad \xi_6 \; ) \tag{4.21}$$

and the decomposed $P^{-1}$ matrix is therefore

$$P^{-1} = T \Lambda T^{-1}. \tag{4.22}$$

where $\Lambda$ is the diagonal matrix of eigenvalues $\lambda_i$ corresponding to $\xi_i$. Taking the least squares equation and bringing the covariance matrix to the left hand side

$$P^{-1} \Delta x = H^T W H. \tag{4.23}$$

Substituting the decomposed matrix and premultiplying each side by $T^{-1}$ produces

$$\Lambda T^{-1} \Delta x = T^{-1} H^T W b. \tag{4.24}$$

Letting $\Delta y = T^{-1} \Delta x$ transforms the state space correction vector into the eigenspace spanned by the vectors of $T$. Upon examining $\Lambda$, there will be a zero eigenvalue and the corresponding element of $\Delta y$ is its contribution to the correction vector in the state space. Setting this element of $\Delta y$ to zero eliminates this contribution, hence transforming this vector

42

back to Δx produces a new correction vector which will produce convergent updates.

Performing this procedure is not without its drawbacks. Since the correction contribution along the slant range vector was nulled, there are many different solutions to the azimuth and elevation data fit. Hence any reasonable input slant range will produce random residuals upon convergence though the slant range derived from the converged solution will not vary much from the input value.

## Range Determination

Based on the data alone, the slant range from the sensor to the target cannot be realized since the information contained in the data set is purely direction with respect to the orbiting platform. The best range estimate one can obtain given the data is from the Gauss method. Even then the analyst must know something about the physics of the problem and the geometry involved. However, there is another inherent piece of information which can be derived from the data -- the rate at which the target passes through the field of view.

Assuming the platforms and objects are in circular co-planar orbits, the angular rate at which satellites revolve about the earth is the mean motion, n, in radians per second,

43

$$n = \omega = \left[\frac{\mu}{a^3}\right]^{1/2} \qquad (4.25)$$

where a is the semimajor axis of the orbit and $\mu$ is the Earth's gravitational parameter. Defining $\omega_g$ as the angular rate of the platform and $a_g$ its semimajor axis, the target angular rate $\omega$ can be expressed in terms of a variation $\delta a$ away from $a_g$, or

$$\omega = \left[\frac{\mu}{(a_g + \delta a)^3}\right]^{1/2} . \qquad (4.26)$$

The above equation can be rewritten in a binomial series in terms of the ratio $\delta a / a_g$

$$\omega = \omega_g \sum_{n=0}^{\infty} \frac{(3/2)_n (-1)^n}{n!} \left[\frac{\delta a}{a_g}\right]^n \qquad (4.27)$$

where the notation $(a)_n$ detotes the Pochhammer operator[*]. Assuming $\delta a$ is much less than $a_g$, the third order series representation is

$$\omega = \omega_g \left(1 - 3/2\alpha + 15/8\alpha^2 - 35/16\alpha^3\right) , \quad \alpha = \delta a / a_g. \qquad (4.28)$$

Therefore the angular rate of the target relative to the sensor is

---

[*]The Pochhammer operator $(a)_n = (a)(a+1)(a+2)...(a+n-1)$.

$$(\omega - \omega_q) = \omega_q \left( - 3/2\alpha + 15/8\alpha^2 - 35/16\alpha^3 \right),$$

$$\alpha = \delta a/a_q. \qquad (4.29)$$

Since both objects are assumed in circular orbits, the radial velocity is equal to zero. This makes the velocity merely the radius times the angular rate in radians per second, or $v = r\omega$. Substituting the semimajor axis for radius makes the velocities become

$$v = \omega \left( a_q + \delta a \right) , \quad v_q = \omega \, a_q \qquad (4.30)$$

and the relative inertial target velocity

$$\delta v = (v - v_q) = a_q \left( \omega + \omega_q \right) - \delta a \, \omega$$

$$= \delta a \, \omega_q \left( - 1/2 + 3/8\alpha - 5/16\alpha^2 + 35/128\alpha^3 \right),$$

$$\alpha = \delta a/a_q. \qquad (4.31)$$

The target position with respect to the platform is given by the vector equation

$$\mathbf{r} = \rho + \mathbf{R},$$

$\mathbf{r}$ being the target, $\mathbf{R}$ the platform and $\rho$ the relative position (slant range) vectors. Since $\rho$ is measured in the sensor coordinate frame, the target velocity $\mathbf{r}'$ becomes

$$\mathbf{r}' = \mathbf{R}' + \rho' + \omega \, \mathbf{X} \, \rho \qquad (4.32)$$

45

where ' indicates the time derivative. Moving $R'$ to the left hand side and expanding $\rho$ into its components,

$$r' - R' = \delta v = \rho' e_r + \rho \beta' e_\theta + \omega e_z \ X \ \rho e_r. \qquad (4.33)$$

The earth subtends approximately 17° at geosynchronous altitude. A simulation of two coplanar circular orbits and determing the relative motion of a lower altitude satellite with respect to a near-geosynchronous satellite has shown that within the viewing cone, the sensor relative aspect angle rate $\beta'$ is constant. Though $\beta'$ is constant, the value of $\beta'$ varies with slant range distance.

Assuming $\rho$ is constant through the field of view, and since $\delta a$ is small, $\rho \approx \delta a$, the relative inertial velocity can be written in terms of tangential components only, or

$$\delta v = \delta a \ ( \ \beta' + \omega \ ). \qquad (4.34)$$

This makes the expression

$$\beta' = \omega_q \ ( \ -3/2 + 3/8\alpha - 5/16\alpha^2 + 35/128\alpha^3 \ ) \ ,$$
$$\alpha = \delta a/a_q \qquad (4.35)$$

which can be solved for $\alpha$ since $\beta'$ is known from the data.

46

## V. Results

Three events were analyzed with the developed program, two of which had single data set collections. The third event was quite unique in that there were four consecutive days worth of data collected on the same object. This multi-day collection was verified by analyzing the intensity profile history for each collection. Each data set had the identical rotation rate, nearly the same intensity level, and started approximately 72 seconds earlier each successive day pinpointing $\delta a$. The focal plane traces are shown in Figure 5. For classification purposes, the single data set events will be designated Event A and Event B. The multiple event will merely be called the multi-day event.

## Event A and B Analysis Results

By analyzing Events A and B, deriving the slant range from the angular rate is plausible only when the ratio $\delta a/a_q$ is sufficiently large. Figure 6 illustrates the simulated relative viewing angle from a spaceborne platform of a co-planar target in a circular orbit. For ranges close to the sensor (within 1000 km), $\beta$ has constant slope $-3/2\omega_q$ within the viewing cone produced by the limb of the earth at geosynchronous altitude (8.5° or .148353 radian half-angle). Figure 7 shows that for small $\delta a/a_q$, $\beta'/\omega_q$ increases linearly with the range ratio $\rho/a_q$ at a rate of .375 to 1
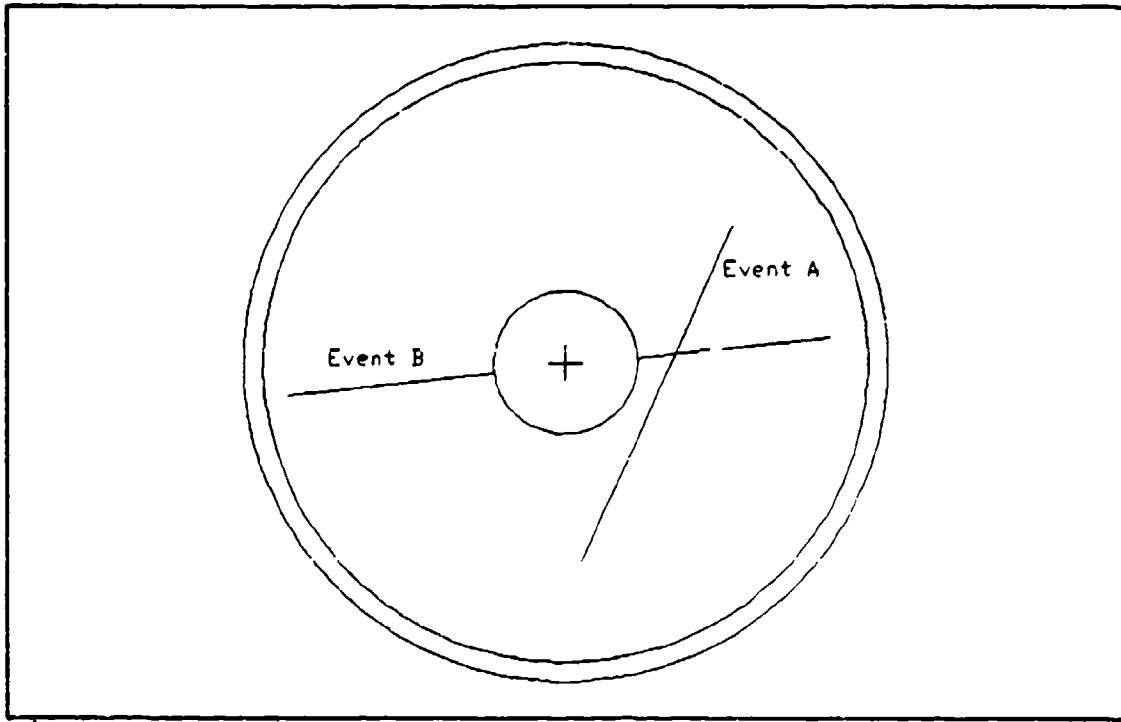
**Figure 5**      Single Data Set Focal Plane Traces

which was expected from the expansion (realistically, $\delta a/a_q \leq$ 0.024, which is an optimistic figure). This means the sum $3/2\omega_q + \beta'$ must lie between -0.008877 and zero to yield a semi-major axis change of less than 1000 km, implying that $\beta' < 0$ since the change in semi-major axis, and hence slant range must be negative due to the equation's derivation (expansion of the quantity $\delta a + a_q$). These constraints on $\beta'$ gave rise to another problem.

The constant term in the series equals 1.09079624 X $10^{-4}$ radians per second, which is approaching the data noise level.

48
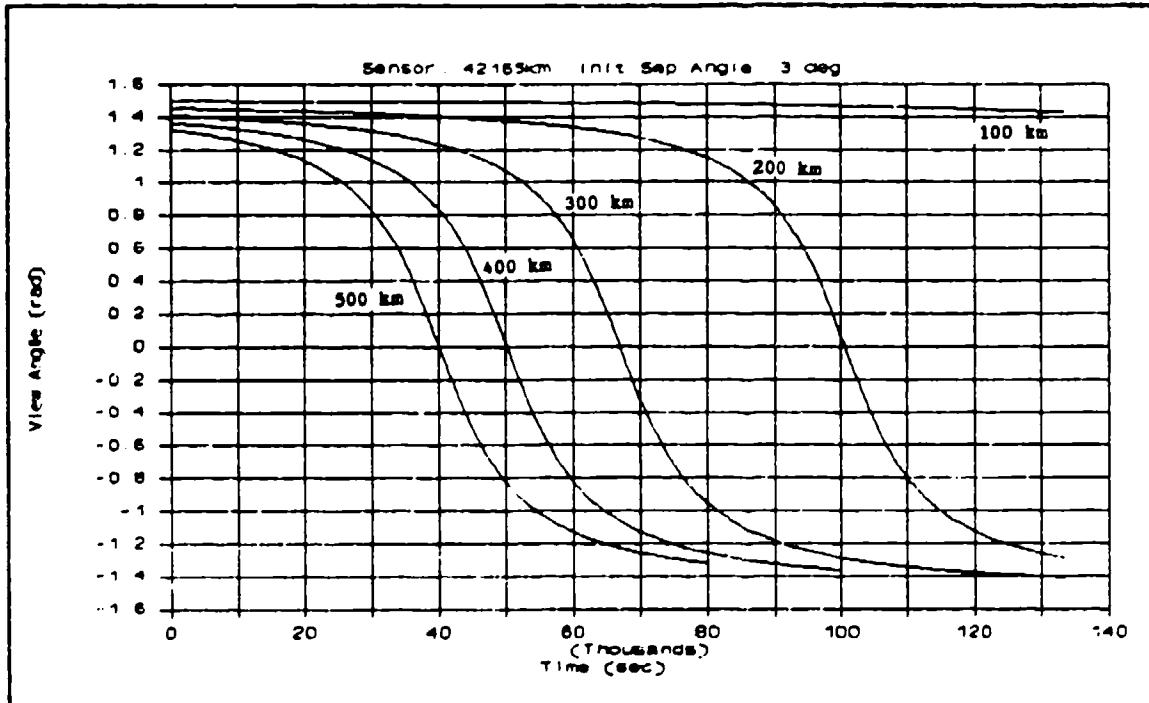
**Figure 6** Simulated View Angle Rates for Various Targets
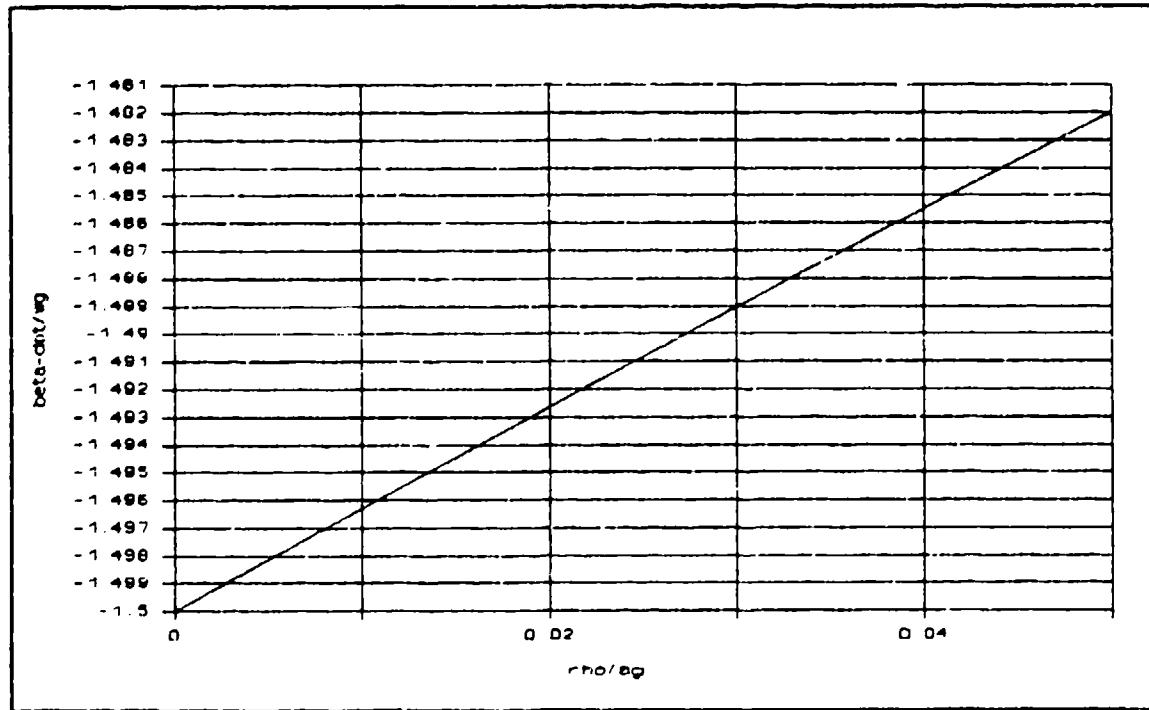


**Figure 7** Actual Angular Rate Ratio vs Range Ratio

49

Hence, the random noise on $\beta'$ easily corrupts the sum $3/2\,\omega_q + \beta'$ producing unreasonable range results since the sum must be multiplied by $8/3a_q$ ($\approx 112645$ km) for a first order approximation. Therefore, the slant range calculation is extremely sensitive to data corruption, making this method of range determination unfeasible. This result is in agreement with Hrastar who concluded that even with three onboard sensors, small uncertainties in target location produces large uncertainties in the range (11:3).

The Gauss orbit determination method worked fairly well for determining an initial orbit and a relationship between $r$ and $v$. Some of the derived range solutions were unrealistic since they produced targets either behind the sensor or too far away to be detected. Noise was a minimal contributor to this problem since the data were smoothed via an analyst supplied $n^{th}$ order least squares polynomial. In fact, changing the polynomial order produced negligible change in the computed radius vector through $3^{rd}$ order.

After fitting the data on these events with an arbitrary slant range, the mean of the residuals was on the same order as the standard deviation, indicating a bias existed. This bias essentially shifted the estimated state vector away from the nominal solution producing unreasonable target selection choices.

50

Each targets' data set, regardless of its size, spans at best approximately 3% of its orbit on a single pass since the target is also near geosynchronous altitude. The slant range, which can be approximated by a change in semi-major axis between the target and sensor, is unknown; only the direction from the sensor at any one time is known given the data. For both of the single set events, the least observable eigen-vector was exactly aligned with the direction cosine vector from the sensor to the target with a near-infinite eigenvalue. Therefore, each slant range chosen by the analyst will fit the data equally well. Figure 8 through Figure 11 show the resid-uals for both Event A and Event B. Table II lists the data fit statistics.

The equinoctial element set was computed from the state vector to avoid the singularities associated with the other element sets. The state vector covariance matrix was also transformed to the equinoctial covariance matrix to determine the uncertainties of each element, with the Jacobian being computed via numerical partials. Unsurprisingly, all of the elements with the exception of the semi-major axis were known. The single data set equinoctial element covariance matrices for a given range are shown in the appendix.

Since the sensor position is assumed exactly known, the smaller the slant range, the smaller the semi-major axis variance, $\sigma_a^2$. Figure 12 shows a higher order growth in the

51
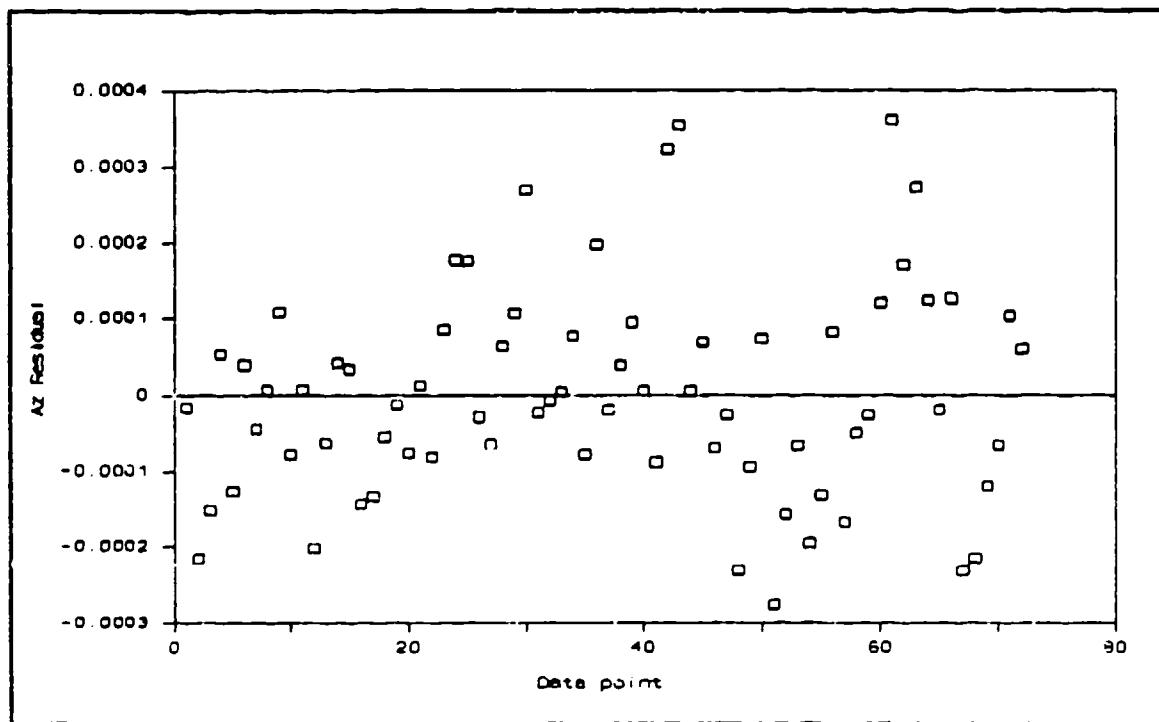
**Figure 8**        Event A Azimuth Residuals
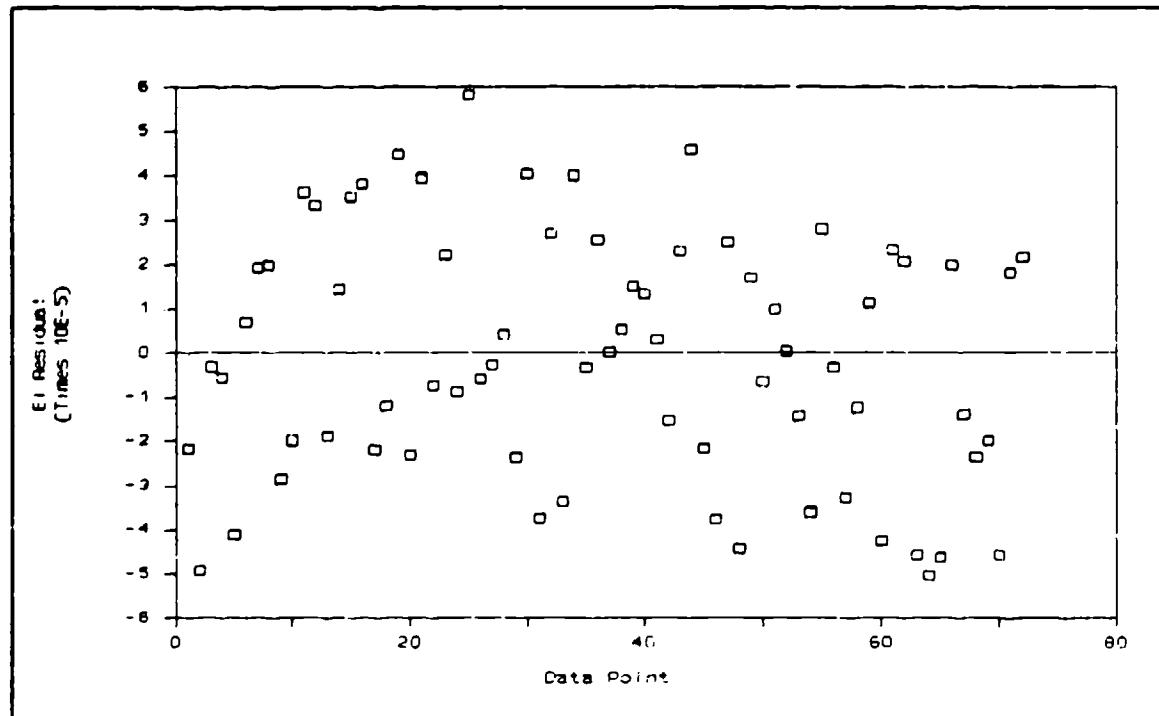


**Figure 9**        Event A Elevation Residuals

52
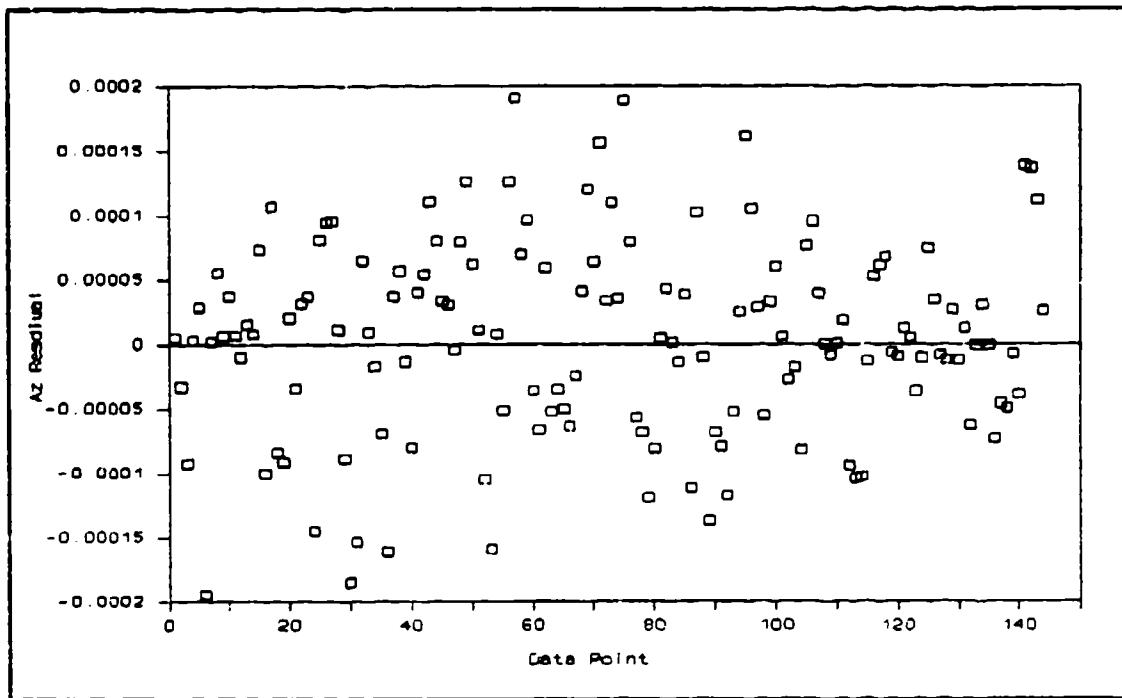
**Figure 10**          Event B Azimuth Residuals
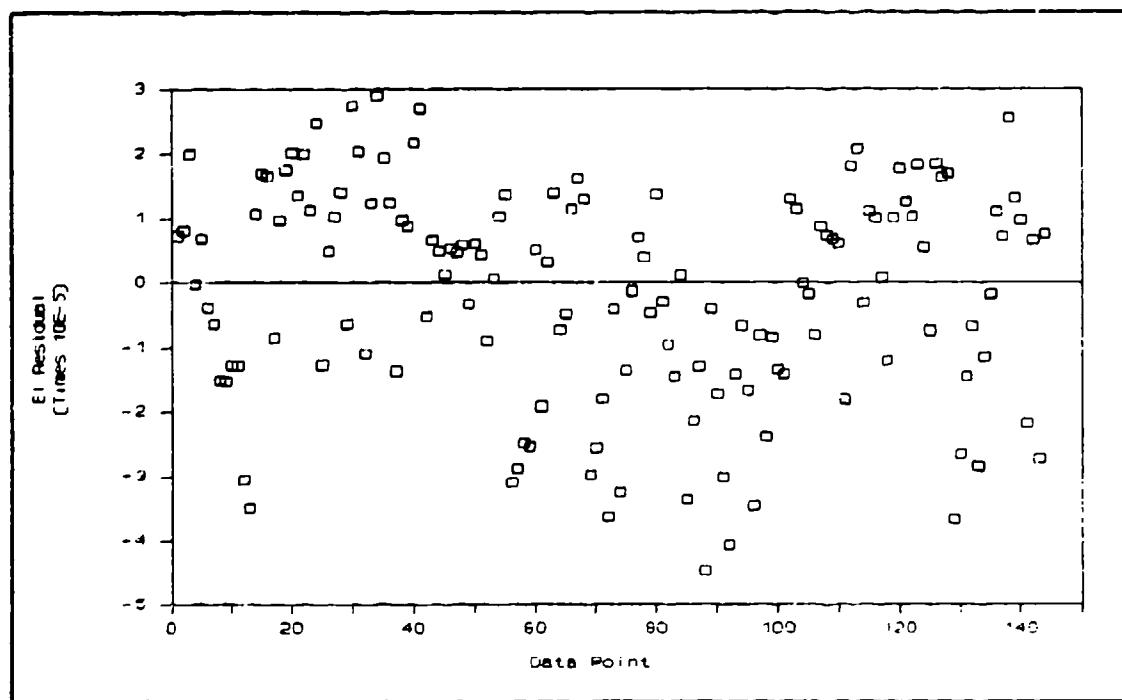


**Figure 11**          Event B Elevation Residuals

53

**Table II**   Single Data Set Event Converged Statistics

|  | Mean | $\sigma$ | RMS |
|---|---|---|---|
| **Event A** | | | |
| Az: | -3.72130E-8 | 1.38461E-4 | 1.37496E-4 |
| El: | -1.04324E-8 | 2.77278E-5 | 2.75345E-5 |
| **Event B** | | | |
| Az: | 1.75770E-6 | 5.25703E-5 | 5.23875E-4 |
| El: | -1.46506E-6 | 1.67384E-5 | 1.66801E-4 |

semi-major axis certainty the further the target is from the sensor. This makes perfectly good sense since $P_2 = \Phi(t_2, t_1) P_1 \Phi(t_2, t_1)^T$. In fact, from this relation, $\sigma_a^2$ should increase in the order of $\rho^4$ at best since $\Phi$ is at most second order.

## Multiple Collection Event

It was quite fortunate that a series of collections on the same object was located in the data base. The target had a periodic intensity profile which repeated itself upon each track, thus ascertaining that it was the same object. Each profile consisted of a series of specular troughs and valleys indicating that it was multisurfaced. A rotation rate could not be derived since the intensity pattern did not repeat over the duration of the track. Figure 13 shows the composite focal plane traces.
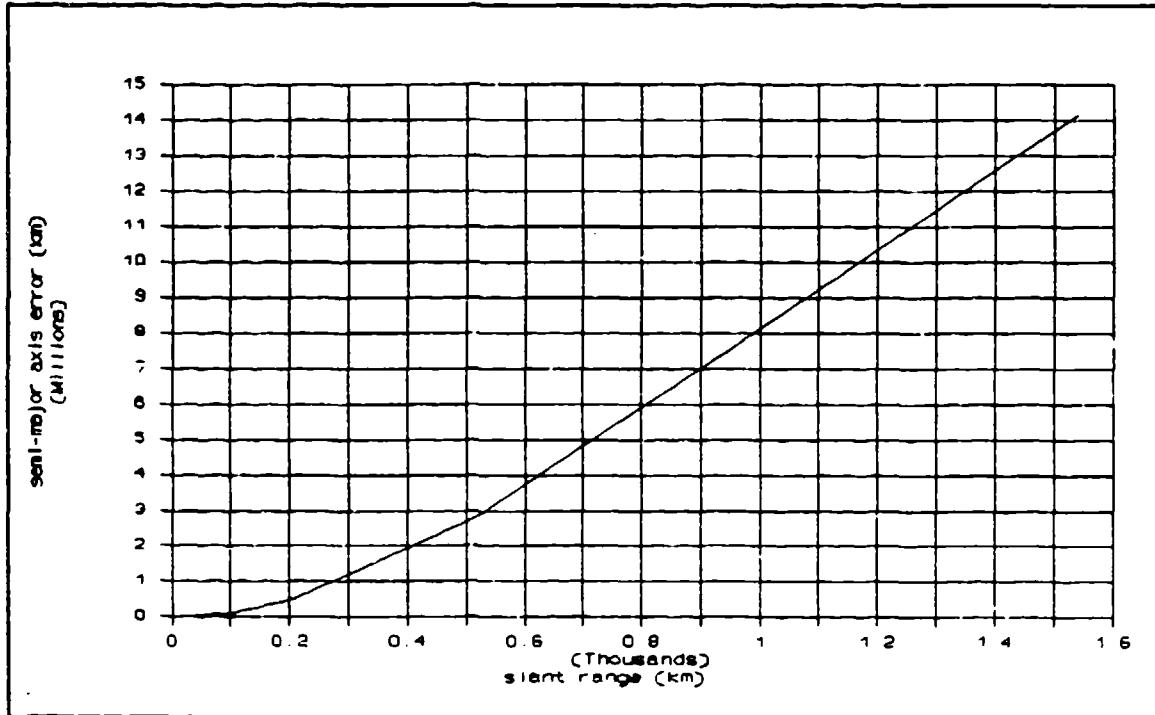
Figure 12   $\sigma_a^2$ vs Slant Range for Single Data Set Events
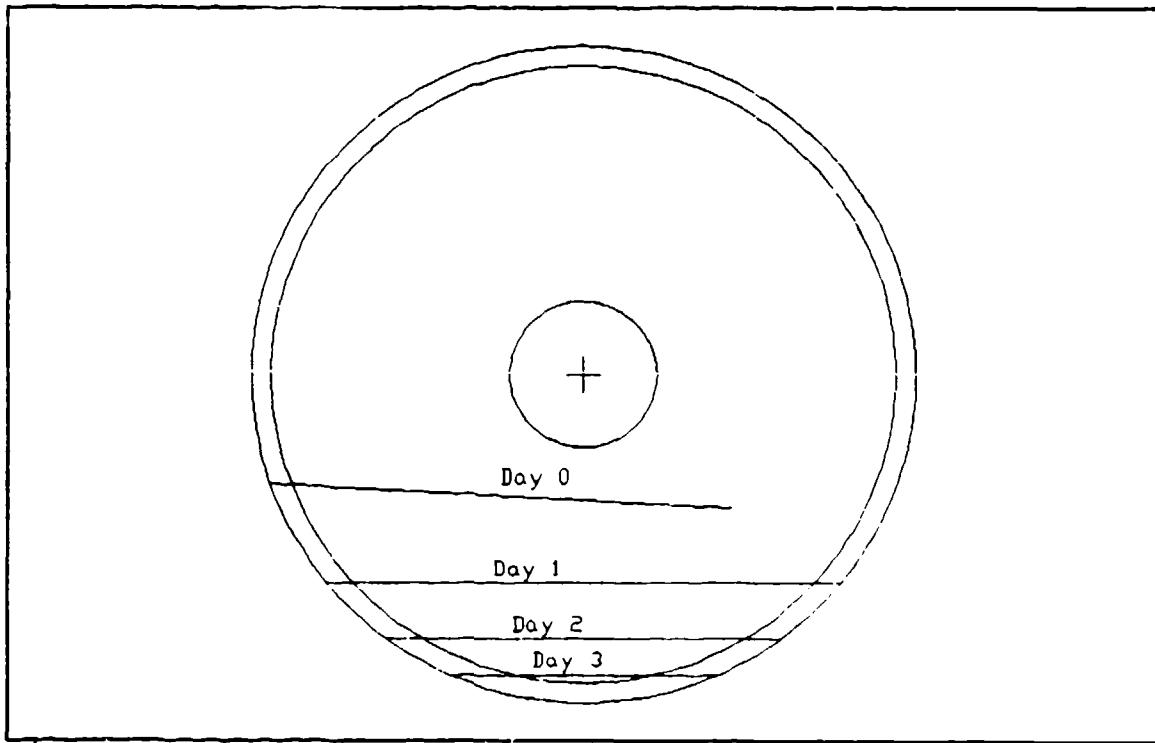


Figure 13      Multi-Day Event Focal Plane Traces

55

Knowing the change in track start times from the previous day would give the analyst an idea of what the target semimajor axis should be based on the sensor period. For this event, the sensor had a period of 1436.154 minutes and each track started approximately 215 seconds earlier each day putting the target 70.5 km away.

Since two body motion was used to propagate both sensor and target state vectors over three days, the integration step size had to be decreased a significant amount (approximately 60 second increments) in order to fit the position ephemerides. This led to long analysis runs, but it was imperative that each succeeding day's sensor ephemerides (given) match the propagated state vector. Also, each data partial had to be related back to the epoch time via the chain rule.

Using the a-priori slant range value, an initial orbit was computed from the Gauss algorithm for the first day's worth of data. A trial and error method was used to find a slant range which would "hit" the next day's data. Though any range would fit data set, only one slant range would fit two data sets collected on the same object. Each latter data set became easier to fit once the first two data sets were fit.

Different subroutines were "turned off" so that the data could drive the covariance matrix calculations. For instance, the eigenvalue/observability check routine was not needed since the covariance matrix was now invertible -- the slant

56

range was now defined. Data partial derivatives were not required between collections. Hence that routine was bypassed until the first data point of the next set was reached.

The entire four data sets were fit using the nominal Gaussian standard deviations listed in the sensor specifications. As expected, the semi-major axis error dropped significantly to within 4 km. The error for the remainder of the elements also was reduced, but not to the extent as the semi-major axis error. Figure 14 and Figure 15 show the multiple day event data fit residuals. Note the end of each data set after careful inspection of the plots.

Table III lists the derived classical element set and the respective element errors. Any element which involves velocity in its computation (i.e. eccentricity, argument of perigee, mean anomaly and semi-major axis) has a higher uncertainty than the pure position derived elements (ascending node and inclination) since error is extremely sensitive to changes in position derivatives.

Once the data was fit, the obtained fastwalker state vector was propagated to find the range at the nadir crossing for each of the four days, shown in Table IV. The target appeared to have drifted approximately 40 km further from the sensor each day for two days and then stopped. This effect was due to the relative changes in the orbit between the sensor and target since the eccentricity is not exactly zero.

57
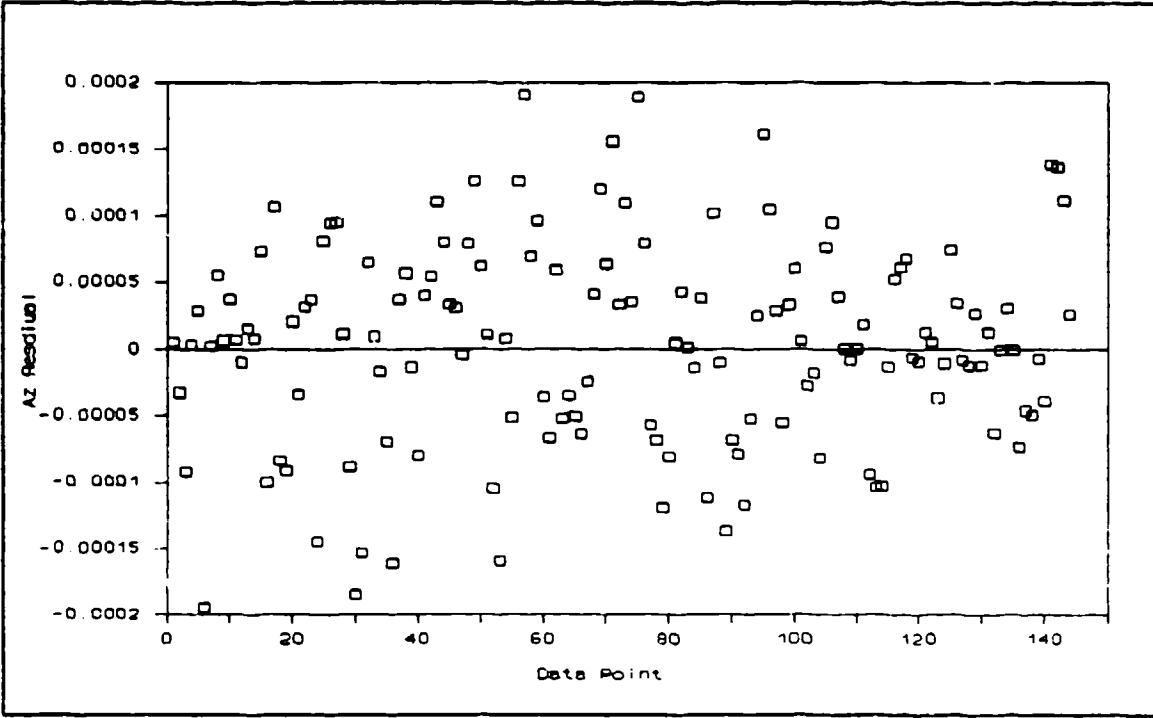
**Figure 14    Multiple Day Event Azimuth Residuals**
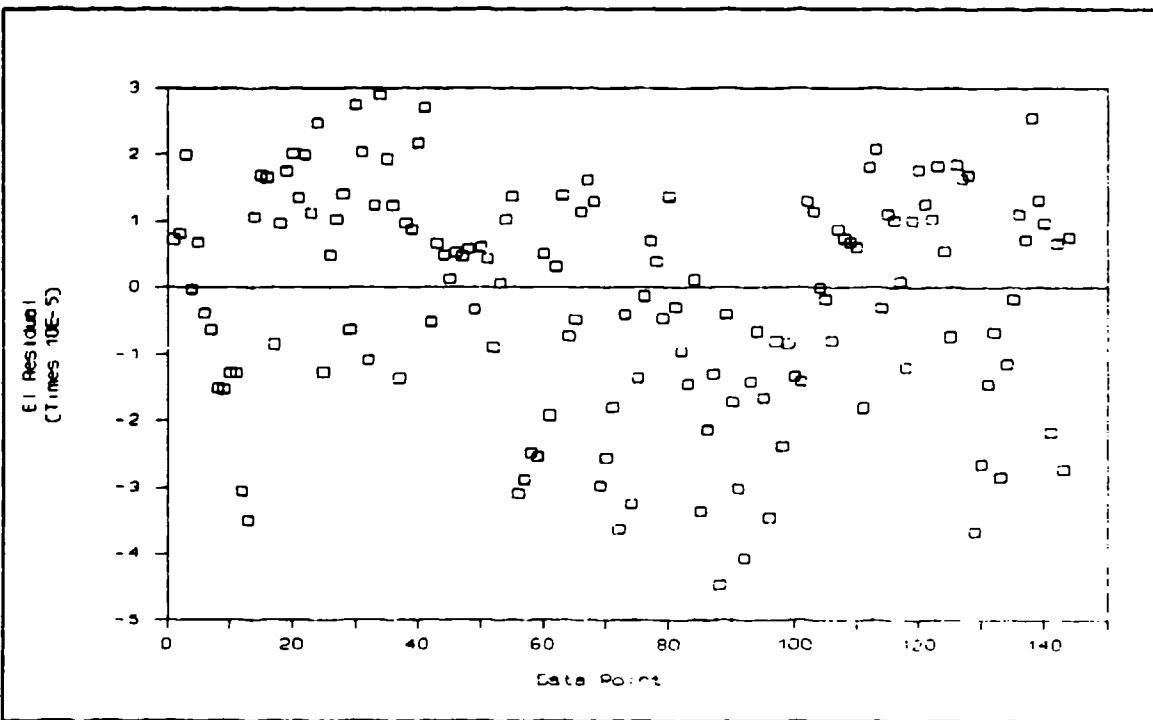


**Figure 15   Multiple Day Event Elevation Residuals**

58

**Table III  Derived Multiple Day Event Results**

```
Semi-major Axis, a        42167.15 km      σ = 3.6 km
Eccentricity, e           .00298           σ = .000213
Inclination, i            5.664°           σ = .000305°
Ascending Node, Ω         70.566°          σ = .000746°
Argument of Perigee, ω    316.800°         σ = .0198°
Mean Anomaly, M           96.489°          σ = .00281°

Azimuth
   Mean: 8.17632E-7       RMS: 4.96381E-5  σ: 4.99205E-5

Elevation
   Mean: 5.61084E-7       RMS: 1.17450E-5  σ: 1.20884E-5
```

**Table IV  Multiple Day Event Nadir Crossing Ranges**

```
Day 0:   79.0 km              Day 2:   176.2 km

Day 1:   130 km              Day 3:   180.4 km
```

59

## VI. Summary and Conclusions

Fastwalker orbit determination cannot be performed with a single data set. Multiple simultaneous collections by different sensors or another sighting by the same sensor on a different day is required to determine the orbital element set with any certainty. Hence any future occurrences with other sensors cannot be computed accurately since errors are also propagated along with the state.

A near-perfect estimate of the sensor position and velocity is required so any errors contributed to the results will be due to the data and not the ephemeris. This is accomplished by assuming the first ephemeris position point is known and fitting the remainder of the position ephemerides by estimating the velocity. This adds confidence to the propagated state vector when fitting multiple day collections.

The Gauss method provides a good initial orbit provided the data does not have any biases (zero mean), especially since the method assumes perfect data. Hence, no error statistics are associated with the elements. Once the eighth-order polynomial is factored, the method occasionally produces possible target ranges where the target would not be detected due to the lower reflected sunlight intensity level or a negative range meaning the target is behind the sensor. These outputs are naturally impossible and the method fails. The

method does however provide a relationship between the target position and velocity vectors as a function of range.

Since the target is essentially coplanar with the sensor, the range is the difference in the target semi-major axis from the sensor. Unfortunately, the least observable eigenvector derived from the covariance matrix is along the line of sight indicating that any range will fit the azimuth and elevation data equally well. The least confident element is the semi-major axis; its error increases as a function of $\rho'$. The balance of the element errors, whether they be classical or equinoctial, increase at a much slower rate. For data sets with n' zero mean, the remainder of the elements are confidently known when the target is within 100 km. Otherwise the errors grow almost as fast as the semi-major axis error.

Multiple sightings on different days require a relatively small integration step if two body motion is to be used for propagating the sensor and initial fastwalker state vectors. The semi-major axis error is significantly reduced with each additional data set. Once two data sets are fit (which is a chore in and of itself), the third and later sets become easier to analyze since the epoch estimate is more refined. The major problem is finding a range which will produce an orbit consistent with the second data set. Perturbations do not play a major role since these effects are insignificant over the time period of the analyzed events and they are also

61

absorbed in the data noise. Though the data residuals still have trends, the RMS values are acceptible given the bias problems.

Care must be taken to ensure that the same object is being tracked else many hours will be wasted. This is done by comparing intensity history patterns of various detected objects. The intensity level is not important since it is a function of the materials used to build the target, location of the sun at the time of collection, target attitude with respect to the sensor and other effects in addition to distance from the sensor. Only the specular pattern is important since most of the satellites in geosynchronous orbit are spinners with despun shelves. This pattern gives the analyst an idea of the target shape and the spin rate. It is similar to a fingerprint -- an identifying trait which discerns one object from another.

# VII. Recommendations

The topic of this thesis has not been deeply investigated by many analysts within the space and intelligence community. It is only recently that fastwalker analysis has become an important issue due to an ever increasing number of geosynchronous satellites and the inability to track and catalog these objects with ground-based sensors. Therefore many related topics are available for research.

The main hurdle to overcome with fastwalker analysis with a single data set is the range ambiguity. Rederiving the Gauss orbit determination method to include state vector error statistics will be able to provide the estimator information about what it is calculating. Since the direction cosine vectors are fit with a least squares polynomial, there is some error information present which could be related to the initial state estimate from the Gauss algorithm. It is possible to transform these error statistics into some type of a-priori covariance matrix which in turn can be added to the least squares covariance matrix. This will control the estimation process iteration and reduce the need to decompose the least squares covariance matrix.

Secondly, devising a method to remove biases from the data will help allow the Gauss method to perform better with the given data thus providing a more confident initial state

63

vector to the estimator. This can be combined with the above recommendation to again furnish the estimator with error statistics about what it is receiving.

Lastly, one can perform intensity history profile comparisons to determine when the same object is detected by two orbiting sensors in different locations. This will involve perturbation theory and propagating state vectors (or orbital elements) over long time periods and then fit two or more data sets. Accurate propagation models using the HAMING integrator will be required (19:B-12).

64

Appendix: <u>Covariance Matrices for Events A and B</u>

The following matrices are typical single data set event covariance matrices. Each matrix is for a specific event and the matrix elements are functions of range and how well the data was fit. The given ranges were derived by the Gauss algorithm. Read the elements from left to right and top to bottom as follows: a, h, k, $\lambda_0$, p, q (i.e. $P_{23}$ is the partial derivative of h with respect to k).

<u>Event A Equinoctial Element Covariance Matrix at $t_0$, $\rho$ = 25km</u>

0.46298E+00 0.36882E-03 0.60340E-03 0.41122E-04 0.12580E-02 0.11407E-02

0.36882E-03 0.29422E-06 0.48127E-06 0.32800E-07 0.10034E-05 0.90989E-06

0.60340E-03 0.48127E-06 0.78739E-06 0.53660E-07 0.16415E-05 0.14885E-05

0.41122E-04 0.32800E-07 0.53660E-07 0.36570E-08 0.11187E-06 0.10144E-06

0.12580E-02 0.10034E-05 0.16415E-05 0.11187E-06 0.34222E-05 0.31032E-05

0.11407E-02 0.90989E-06 0.14885E-05 0.10144E-06 0.31032E-05 0.28140E-05

<u>Event B Equinoctial Element Covariance Matrix at $t_0$, $\rho$ = 425km</u>

0.20772E+07 0.87512E+01 0.58293E+01 0.32037E+01 0.21847E+02-0.56257E+02

0.87512E+01 0.37038E-04 0.24631E-04 0.13496E-04 0.92037E-04-0.23700E-03

0.58293E+01 0.24631E-04 0.16394E-04 0.89899E-05 0.61306E-04-0.15787E-03

0.32037E+01 0.13496E-04 0.89899E-05 0.49410E-05 0.33694E-04-0.86766E-04

0.21847E+02 0.92037E-04 0.61306E-04 0.33694E-04 0.22977E-03-0.59168E-03

-0.56257E+02-0.23700E-03-0.15787E-03-0.86766E-04-0.59168E-03 0.15236E-02

## Bibliography

1.  Bate, R.R. et al. *Fundamentals of Astrodynamics*, Dover Publications, Inc., New York, 1971.

2.  Battin, Richard. *An Introduction to the Mathematics and Methods of Astrodynamics*, Wiley & Sons, Mar 1988.

3.  Conte, S.D. *Elementary Numerical Analysis*, McGraw-Hill Book Company, New York, 1980.

4.  Cefola, Paul. *Equinoctial Orbit Elements - Application to Artificial Satellite Orbits*. AIAA Paper 72-937 presented at the AIAA/AAS Astrodynamics Conference, Palo Alto, CA, September 11-12, 1972.

5.  Day, Kenton. *Trajectory Reconstruction by the Method of Weighted Least Squares*, Report No. SYA-06, Signal Sciences, Inc., Santa Clara, CA, 8 Oct 76.

6.  Escobal, Pedro R. *Methods of Orbit Determination*, Robert E. Krieger Publishing Co., Malabar, FL, 1965.

7.  Ferguson, Jack R. Lecture Notes for ASTRO 453, Advanced Astrodynamics, United States Air Force Academy, CO, 1980.

8.  Geodynamics Corporation, "MVS/TRP Milestone 2/3 Report: Estimation Convergence Criteria," March 1984.

9.  Geodynamics Corporation, "MVS/TRP Milestone 2/3 Report: SENSM Module Equation Logic," March 1984.

10. Greenwood, Donald. *Principles of Dynamics*, Prentice-Hall, Inc., Englewood Cliffs, New Jersey, 1965.

11. Hrastar, John. "Estimation of the Length and Orientation of the Line Between Two Closely Co-orbiting Satellites," *Journal of Spacecraft and Rockets*, Vol 7, No 10, October 1970.

12. Junkins, J.L. *An Introduction to Optimal Estimation of Dynamical Systems*, Sistoff and Nordoff Publishers, The Netherlands, 1978.

13. Kaplan, Marshall. *Modern Spacecraft Dynamics and Control*, John Wiley & Sons, New York, 1976.

14. -----. Seminar Notes for Satellite Orbit and Attitude Control Systems, George Washington University, 1986.

15. Kreysig, Edwin. *Advanced Engineering Mathematics*, Sixth Edition, John Wiley & Sons, 1988.

16. Lillard, Larry N. *Post Flight Trajectory Reconstruction of a Maneuvering Reentry Vehicle from Radar Measurements*, M.S. Thesis, Air Force Institute of Technology, Wright-Patterson AFB, OH, Dec 1982.

17. Mierovitch, L. *Methods of Analytical Dynamics*, McGraw-Hill Book Company, New York, 1970.

18. Toines, C.C. *et al*. *TRACE Orbit Determination Program Version D*, Report No TR-669(9990)-3, Aerospace Corporation, September 1966.

19. Wiesel, William. Lecture Notes for MC 7.31, Modern Methods of Orbit Determination, Air Force Institute of Technology, Wright-Patterson AFB, OH, 1988.

20. Wolaver, L.E. *Modern Techniques in Astrodynamics -- An Introduction*, Defense Technical Information Center, Alexandria, VA, December 1970 (AD 718963).

21. Wong, Lem. *Fastwalker Orbit Determination*, Aerospace Corporation Technical Report 85-34531, El Segundo, CA, 1985.

## Vita

Captain Richard P. Osedacz was born on 24 February 1962 in Central Falls, Rhode Island. He graduated from high school in Cumberland, Rhode Island in 1980 and attended the United States Air Force Academy from which he received the degree of Bachelor of Science in Astronautical Engineering in May 1984. Upon graduation he received a regular commission in the USAF and was assigned to the Foreign Technology Division, Directorate of MASINT Exploitation, Powered Flight Performance Group where he spent the next three years as a ballistic missile performance engineer. In 1987 he served as Deputy Branch Chief, Powered Flight Performance Group until entering the School of Engineering, Air Force Institute of Technology, in May 1988.

> Permanent Address: 44 E. Earle St
> Cumberland, RI 02864

| REPORT DOCUMENTATION PAGE | | Form Approved OMB No. 0704-0188 |
|---|---|---|

| 1a. REPORT SECURITY CLASSIFICATION UNCLASSIFIED | 1b. RESTRICTIVE MARKINGS |
|---|---|
| 2a. SECURITY CLASSIFICATION AUTHORITY | 3. DISTRIBUTION/AVAILABILITY OF REPORT |
| 2b. DECLASSIFICATION/DOWNGRADING SCHEDULE | |

| 4. PERFORMING ORGANIZATION REPORT NUMBER(S) AFIT/GA/ENY/89J-3 | 5. MONITORING ORGANIZATION REPORT NUMBER(S) |
|---|---|

| 6a. NAME OF PERFORMING ORGANIZATION School of Engineering | 6b. OFFICE SYMBOL (If applicable) AFIT/ENY | 7a. NAME OF MONITORING ORGANIZATION |
|---|---|---|
| 6c. ADDRESS (City, State, and ZIP Code) Air Force Institute of Technology Wright-Patterson AFB OH 45433-6583 | | 7b. ADDRESS (City, State, and ZIP Code) |

| 8a. NAME OF FUNDING/SPONSORING ORGANIZATION Flight Performance Division | 8b. OFFICE SYMBOL (If applicable) FTD/SQDF | 9. PROCUREMENT INSTRUMENT IDENTIFICATION NUMBER |
|---|---|---|

| 8c. ADDRESS (City, State, and ZIP Code) HQ Foreign Technology Division Wright-Patterson AFB OH 45433 | 10. SOURCE OF FUNDING NUMBERS | | | |
|---|---|---|---|---|
| | PROGRAM ELEMENT NO. | PROJECT NO. | TASK NO | WORK UNIT ACCESSION NO. |

**11. TITLE (Include Security Classification)**
ORBIT DETERMINATION OF SUNLIGHT_ILLUMINATED OBJECTS DETECTED BY OVERHEAD PLATFORMS

**12. PERSONAL AUTHOR(S)**
Richard P. Osedacz, B.S., Capt, USAF

| 13a. TYPE OF REPORT MS Thesis | 13b. TIME COVERED FROM _____ TO _____ | 14. DATE OF REPORT (Year, Month, Day) 1989 June | 15. PAGE COUNT 78 |
|---|---|---|---|

**16. SUPPLEMENTARY NOTATION**

| 17. | COSATI CODES | | 18. SUBJECT TERMS (Continue on reverse if necessary and identify by block number) |
|---|---|---|---|
| FIELD | GROUP | SUB-GROUP | Orbit Determination    Angle-only data |
| 22 | 03 | | Fastwalkers |
| | | | |

**19. ABSTRACT (Continue on reverse if necessary and identify by block number)**

Thesis Advisor: William E. Wiesel
          Professor
          Department of Aeronautics and Astronautics

| 20. DISTRIBUTION/AVAILABILITY OF ABSTRACT ☒ UNCLASSIFIED/UNLIMITED ☐ SAME AS RPT. ☐ DTIC USERS | 21. ABSTRACT SECURITY CLASSIFICATION UNCLASSIFIED | |
|---|---|---|
| 22a. NAME OF RESPONSIBLE INDIVIDUAL William E. Wiesel, Professor | 22b. TELEPHONE (Include Area Code) 513-255-3517 | 22c. OFFICE SYMBOL ENY |

**DD Form 1473, JUN 86**          *Previous editions are obsolete.*          SECURITY CLASSIFICATION OF THIS PAGE

A technique for determining the orbital element set of a sunlight-illuminated object detected by an overhead platform (when passing through the sensor's field of view) is developed. The technique uses a Gauss orbit determination technique to find an initial target state estimate and then the estimate is refined via a batch weighted least squares estimation routine. A six element state vector consisting of three position and three velocity components describe the state at epoch. It was found that the Gaussian method produced reasonable initial orbits when the data bias was sufficiently zero. Each analyst-supplied slant range fit the data equally well, indicating that orbit determination is impossible with a single set of data. A unique series of events where the same object was tracked four consecutive days was fit using the developed algorithm, producing favorable results. The results of two single data set events and one multiple collection events are presented. *Keywords: flight paths; orbits; trajectories; orbit determination; Military targets, (u)*